A Cryptochrome adopts distinct moon- and sunlight states and functions as moonlight interpreter in monthly oscillator entrainment

Short title: Moonlight sets a monthly clock via L-Cry

Birgit Poehn*[1,2], Shruthi Krishnan*[3], Martin Zurl[1,2], Aida Coric[#1,2], Dunja Rokvic[#1,2], Enrique Arboleda[1,2,4], Lukas Orel[1,2], Florian Raible[1,2], Eva Wolf[@3] and Kristin Tessmar-Raible[@1,2]

[1]Max Perutz Labs, University of Vienna, Vienna BioCenter, Dr. Bohr-Gasse 9/4, 1030 Vienna

[2]Research Platform "Rhythms of Life", University of Vienna, Vienna BioCenter, Dr. Bohr-Gasse 9/4, A-1030 Vienna

[3] Structural Chronobiology, Institute of Molecular Physiology (IMP) and Institute of Molecular Biology (IMB) Mainz, Ackermannweg 4, 55128 Mainz, Germany.

[4] present address: Institut de Génomique Fonctionnelle de Lyon (IGFL), École Normale Supérieure de Lyon, 32 avenue Tony Garnier, 69007 Lyon, France

[*,#] equal contribution

[@] correspondence:

Eva Wolf: evawolf1@uni-mainz.de

Kristin Tessmar-Raible: kristin.tessmar@mfpl.ac.at

Abstract

Measuring time by the moon's monthly cycles is a wide-spread phenomenon and crucial for successful reproduction in countless marine organisms. In several species, such as the mass-spawning bristle worm *Platynereis dumerilii*, an endogenous monthly oscillator synchronizes reproduction to specific days. Classical work showed that this oscillator is set by full moon. But how do organisms recognize this specific moon phase?

We uncover L-Cry's involvement: photoreduction and recovery kinetics of its co-factor FAD differ strongly when purified L-Cry is exposed to naturalistic moonlight, naturalistic sunlight, or their different successions. L-Cry's sun- versus moonlight states correlate with distinct sub-cellular localizations, indicating differential signalling. These properties enable a discrimination between sun- and moonlight, as well as moonlight duration as a moon phase indicator.

Consistently, *l-cry* mutants re-entrain their circalunar phase less well than wild-type to naturalistic moonlight. But under artificially strong nocturnal light, *l-cry* mutants re-entrain faster than wildtype, suggesting that L-Cry at least partly blocks "wrong" light from impacting on this oscillator. Our work provides a new level of functional understanding of moon-regulated biological processes.

Main text

The moon fascinates biologists and non-biologists alike. An impact of lunar light on the nervous system, and ultimately on the behavior and metabolism of animals, may at first seem eccentric to modern scientists. But as a matter of fact, lunar influences on animals are especially well documented in the marine environment (*1-3*). Starting with the early 20th century, numerous scientific studies have shown that the reproductive behavior and sexual maturation of animals as diverse as corals, polychaetes, echinoderms, fishes or turtles are synchronized by the lunar cycle (*1, 3-7*). A recent study suggests that the lunar cycle coordinates the behaviour of a nocturnal migratory bird (*8*), and recently uncovered clear correlations of human sleep and menstrual cycle properties with moon phases have re-initiated the discussion of an impact of the moon even on human biology (*9, 10*). In animals, these synchronizations are not only impressive, but typically also important to ensure successful reproduction (*11*). In turn, desynchronization of these reproductively critical rhythms due to anthropogenic disturbances, as documented for corals, poses a threat to species survival (*11*).

Despite the importance and widespread occurrence of lunar rhythms, any functional mechanistic insight is lacking. Importantly, this synchronization among conspecifics is in many cases not simply a direct reaction to a stimulus, but instead governed by endogenous monthly oscillators: circalunar clocks (*3, 12-16*). The marine bristle worm *Platynereis dumerilii* is well-documented to possess such a circalunar clock, which controls its reproductive timing and can be entrained by nocturnal light in the lab (*5, 14, 17*). Several reports have linked the expression of cryptochromes (CRYs) with moon phase, suggesting that these genes could be involved in circalunar time-keeping (*18*), possibly- as proposed for corals- as lunar light receptors (*2, 19, 20*). However, no functional molecular support for such an involvement exists. In order to move from expression correlation to a mechanistic understanding, we investigated the biochemical properties and functional role of the light-receptive cryptochrome L-Cry in the annelid *Platynereis dumerilii* (*14*).

L-Cry responds to naturalistic moonlight by cumulative photoreduction

While we have previously shown that *Pdu*-L-Cry is degraded upon light exposure in S2 cell culture (*14*), it has remained unclear if L-Cry has the spectral properties and sensitivity to sense moonlight and whether this would differ from sunlight sensation. To test this, we purified full-length L-Cry from insect cells (figs. S1A-C). Multiangle light scattering (SEC-MALS) analyses of purified dark-state L-Cry revealed a molecular weight of 133 kDa, consistent with the predicted molecular homodimer weight of 135 kDa (Fig. 1A). Purified L-Cry binds Flavin Adenine Dinucleotide (FAD) as its chromophore (figs. S1D,E). We then used UV/Vis absorption spectroscopy to analyze the FAD photoreaction of L-Cry. The

absorption spectrum of dark-state L-Cry showed maxima at 450nm and 475nm, consistent with the presence of oxidized FAD (fig. S1F, black line).

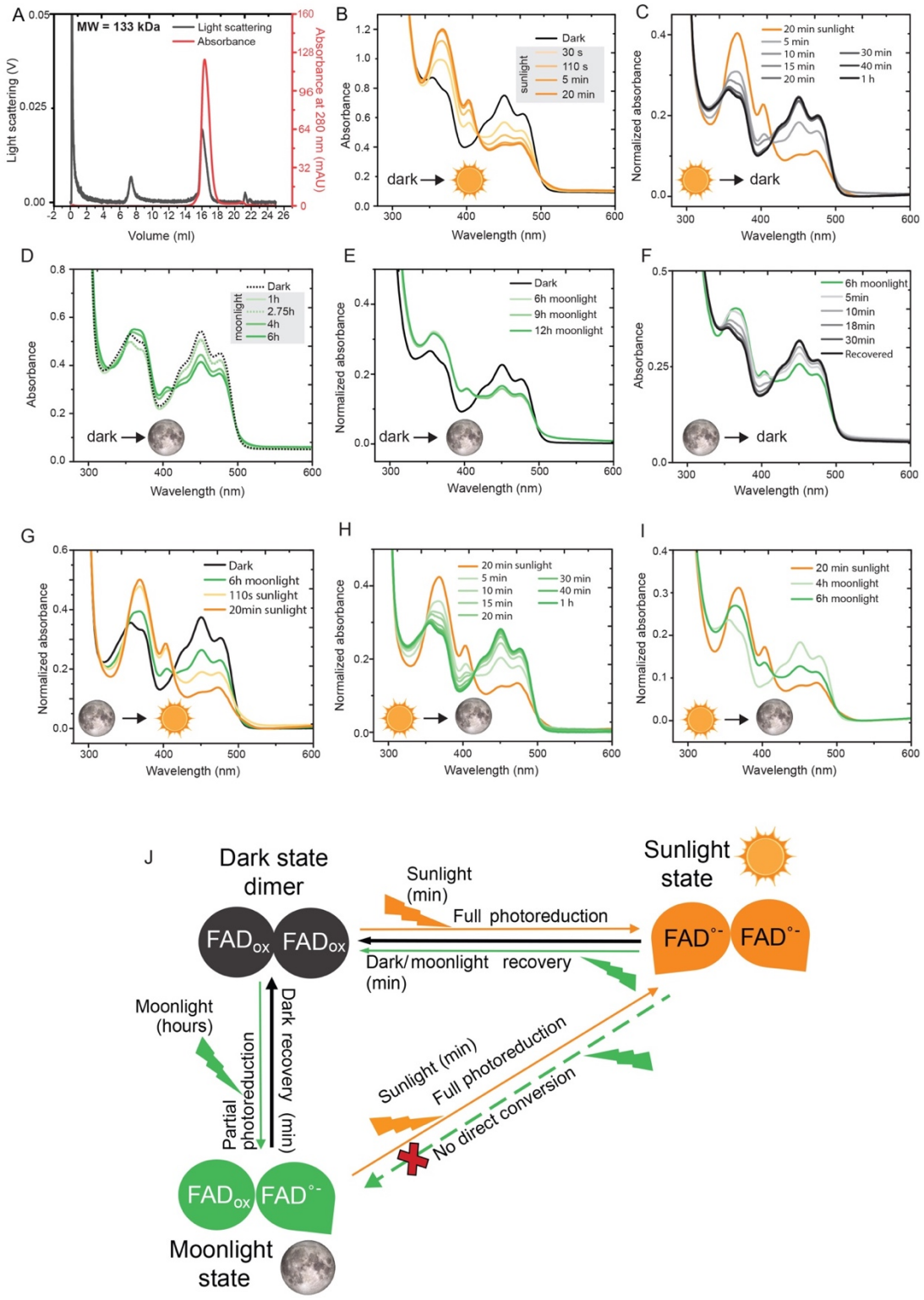

Figure 1*: L-Cry is differently photoreduced by sunlight and moonlight.*
(A) Multi-Angle Light Scattering (MALS) analyses of dark-state L-Cry supports L-Cry homodimer formation (theoretical MW 135 kDa). **(B)** Absorption spectrum of L-Cry in darkness (black) and after sunlight exposure (orange). Additional timepoints: S2A. **(C)** Dark recovery of L-Cry after 20min sunlight on ice. Absorbance at 450nm in S2B **(D,E)** Absorption spectra of L-Cry after exposure to naturalistic moonlight for different durations. **(F)** Full spectra of dark recovery after 6h moonlight. Absorbance at 450nm: S2D. **(G)** Absorption spectrum of L-Cry after 6h of moonlight followed by 20min of sunlight. **(H)**

Absorption spectrum of L-Cry after 20min sunlight followed by moonlight first results in dark-state recovery. Absorbance at 450nm: S2E. **(I)** Absorption spectrum of L-Cry after 20min sunlight followed by 4h and 6h moonlight builds up the moonlight state. **(J)** Schematic model of *Pdu* L-Cry responses to sun- and moonlight. MALS data (A) and preliminary SAXS analyses (data not shown) suggest that L-Cry forms homodimers in its dark and sunlight states, also see discussion and fig. S2I.

As basic starting point to analyze its photocycle, L-Cry was photoreduced with a 445nm emitting strong blue light LED (fig. S3D) for 110s (*21*). The light-activated spectrum showed that blue-light irradiation of L-Cry leads to the complete conversion of FAD_{ox} into an anionic FAD radical (FAD^{o-}) with characteristic FAD^{o-} absorption maxima at 370 nm and 404 nm and reduced absorbance at 450 nm (fig. S1F, blue spectrum, black arrows). In darkness, L-Cry reverted back to the dark state with time constants of 2 min (18°C), 4 min (6°C) and 4.7 min (ice) (figs. S1G-K).

We then investigated the response of L-Cry to ecologically relevant light, i.e. sun- and moonlight using naturalistic sun- and moonlight devices we designed based on light measurements at the natural habitat of *Platynereis dumerilii* (*22*) (figs. S3A,C,E). Upon naturalistic sunlight illumination, FAD was photoreduced to $FAD^{\circ-}$, but with slower kinetics than under the blue light source, likely due to the intensity differences between the two lights (figs. S3C-E). While blue-light illumination led to a complete photoreduction within 110s (fig. S1F), sunlight-induced photoreduction to $FAD^{\circ-}$ was completed after 20 min (Fig. 1B) and did not further increase upon continued illumation for up to 2h (fig. S2A). Dark recovery kinetics had time constants of 3.2min (18°C) and 5min (ice) (Fig.1C, fig. S2B,C).

As the absorbance spectrum of L-Cry overlaps with that of moonlight at the *Platynereis* natural habitat (figs. S3A), L-Cry has the principle spectral prerequisite to sense moonlight. However, the most striking characteristic of moonlight is its very low intensity (1.79 x 10^{10} photons/cm^2/s at -5m, figs. S3A,E). To test if *Pdu*-L-Cry is sensitive enough for moonlight, we illuminated purified L-Cry with our custom-built naturalistic moonlight, closely resembling full moon light intensity and spectrum at the *Platynereis* natural habitat (figs. S3A,C,E). Naturalistic moonlight exposure up to 2.75 hours did not markedly photoreduce FAD, notably there was no difference between 1 hours and 2.75 hours (Fig. 1D). However, further continuous naturalistic moonlight illumination of 4h and longer resulted in significant changes (Fig. 1D), whereby the spectrum transitioned towards the light activated state of FAD^{o-} (note peak changes at 404nm and at 450nm). This photoreduction progressed further until 6 h naturalistic moonlight exposure (Fig. 1D,E). No additional photoreduction could be observed after 9 h and 12 h of naturalistic moonlight exposure (Fig.1E), indicating a distinct state induced by naturalistic moonlight that reaches its maximum after ~6hrs, when about half of the L-CRY molecules are photoreduced. This time of ~6hrs is remarkably consistent with classical work showing that an additional 6hr of nocturnal light period are important for circalunar clock entrainment, irrespective of the preceding photoperiod (*5*). The dark recovery of L-Cry after 6 h moonlight exposure occurred with a time constant of 6.7 min at 18°C (Fig. 1F, fig. S2D). Given that both sunlight and moonlight

117 cause FAD photoreduction, but with different kinetics and apparent different final $FAD^{\circ-}$
118 product/FAD_{ox} adduct ratios, we wondered how purified L-Cry would react to transitions between
119 naturalistic sun- and moonlight (i.e. during “sunrise” and “sunset”).

120 Mimicking the sunrise scenario, L-Cry was first illuminated with naturalistic moonlight for 6 h
121 followed by 20 min of sunlight exposure. This resulted in an immediate enrichment of the $FAD^{\circ-}$ state
122 (Fig. 1G). Hence, naturalistic sunlight immediately photoreduces remaining oxidized flavin molecules,
123 that are characteristic of moonlight activated L-CRY, to $FAD^{\circ-}$, to reach a distinct fully reduced
124 sunlight state.

125 In contrast, when we next mimicked the day-night transition (“sunset”) by first photoreducing with
126 naturalistic sunlight (or strong blue light) and subsequently exposed L-Cry to moonlight, L-Cry first
127 returned to its full dark state within about 30 min (naturalistic sunlight: τ=7min (ice): Fig.1H, fig.S2E;
128 blue light: τ=9 min (ice): fig. S2F-H), despite the continuous naturalistic moonlight illumination.
129 Prolonged moonlight illumination then led to the conversion of dark-state L-Cry to the “moonlight
130 state” (Fig. 1I, fig. S2F), i.e. fully photoreduced “sunlight- state” L-Cry first has to return into the dark
131 state before entering the “moonlight- state” characterized by the stable presence of the partial $FAD^{\circ-}$
132 product/FAD_{ox} adduct. In contrast to “sunlight- state” L-Cry, “moonlight-state” L-Cry does not return
133 to the oxidized (“dark”) state under naturalistic moonlight. Taken together, these results indicate the
134 existance of kinetically and structurally distinct “sunlight” and “moonlight” states of L-Cry (Fig.1J,
135 S2I).

136 Naturalistic sun- and moonlight differently affect L-Cry subcellular 137 localization

138 To further study the function of L-Cry in *Platynereis*, we generated two *l-cry* mutant alleles (Δ34 and
139 Δ11bp) (Fig.2A) using TALENS (*23*), as well as a monoclonal antibody against *Pdu*-L-Cry. Using the
140 mutant worms, we first verified the specificity of the anti-L-Cry antibody in Western blot (Fig. 2B) and
141 immunohistochemistry (Fig. 2E-J). Furthermore, we verified that the staining of the antibody in
142 wildtype worms (Fig. 2E-H) matches the regions where *l-cry* mRNA is expressed (Fig. 2D). These tests
143 confirmed the absence of L-Cry protein in mutants and the specificity of the anti-L-Cry antibody.

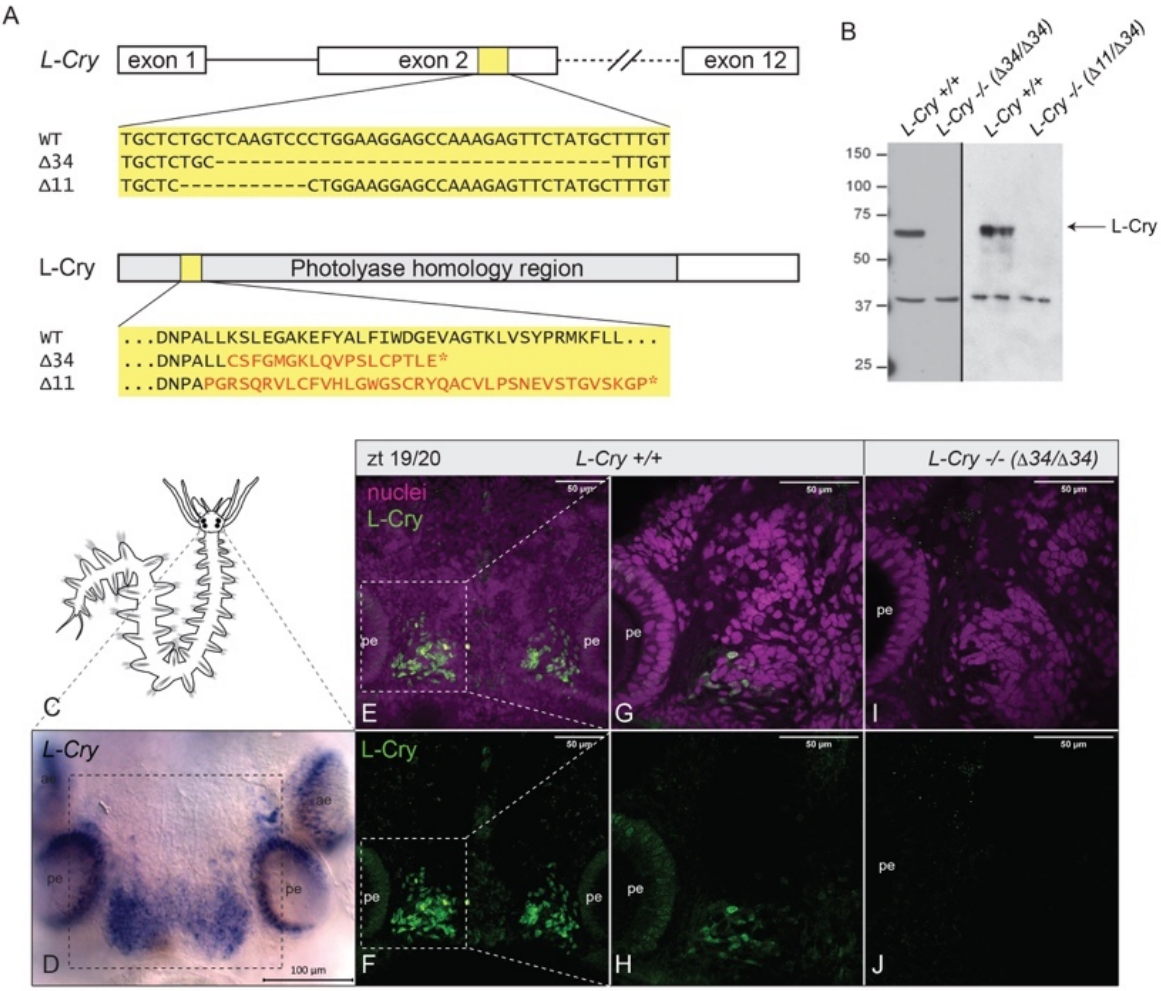

Figure 2. *l-cry -/-* mutants are loss-of-function alleles
(A) Scheme of the *L-Cry* genomic locus for wt and mutants. Both mutant alleles result in an early frameshift and premature stop codon. The Δ34 allele has an additional 9bp deletion in exon 3. **(B)** Western Blots of *P. dumerilii* heads probed with anti-L-Cry antibody. **(C)** scheme of *P. dumerilii.* **(D)** whole mount *in situ* hybridization against *l-cry* mRNA on worm head. ae, anterior eye; pe, posterior eye. **(E-J)** Immunohistochemistry of premature wildtype (E,F,G,H) and mutant (I,J) worm heads sampled at zt19/20 using anti-L-Cry antibody (green) and Hoechst staining (magenta), dorsal views, anterior up. E,F: z-stack images (maximal projections of 50 layers, 1.28µm each) in the area highlighted by the rectangle in (D), whereas (G-J) are single layer images of the area highlighted by the white rectangles in (E) and (F).

In order to further investigate the response of L-Cry to naturalistic sun- and moonlight, we conducted Western blots and immunohistochemistry at different lunar and daily timepoints (Figs. 3A-A''). L-Cry levels after 8h of naturalistic sunlight (day before full moon = FM-1, diel time: zeitgeber time 8 = zt8, Figs. 3A,A') were significantly reduced compared to 8h under darkness at the same moon phase (FM-1, zt 24, Figs. 3B,C), in line with (canonical) L-Cry degradation in response to naturalistic sunlight.

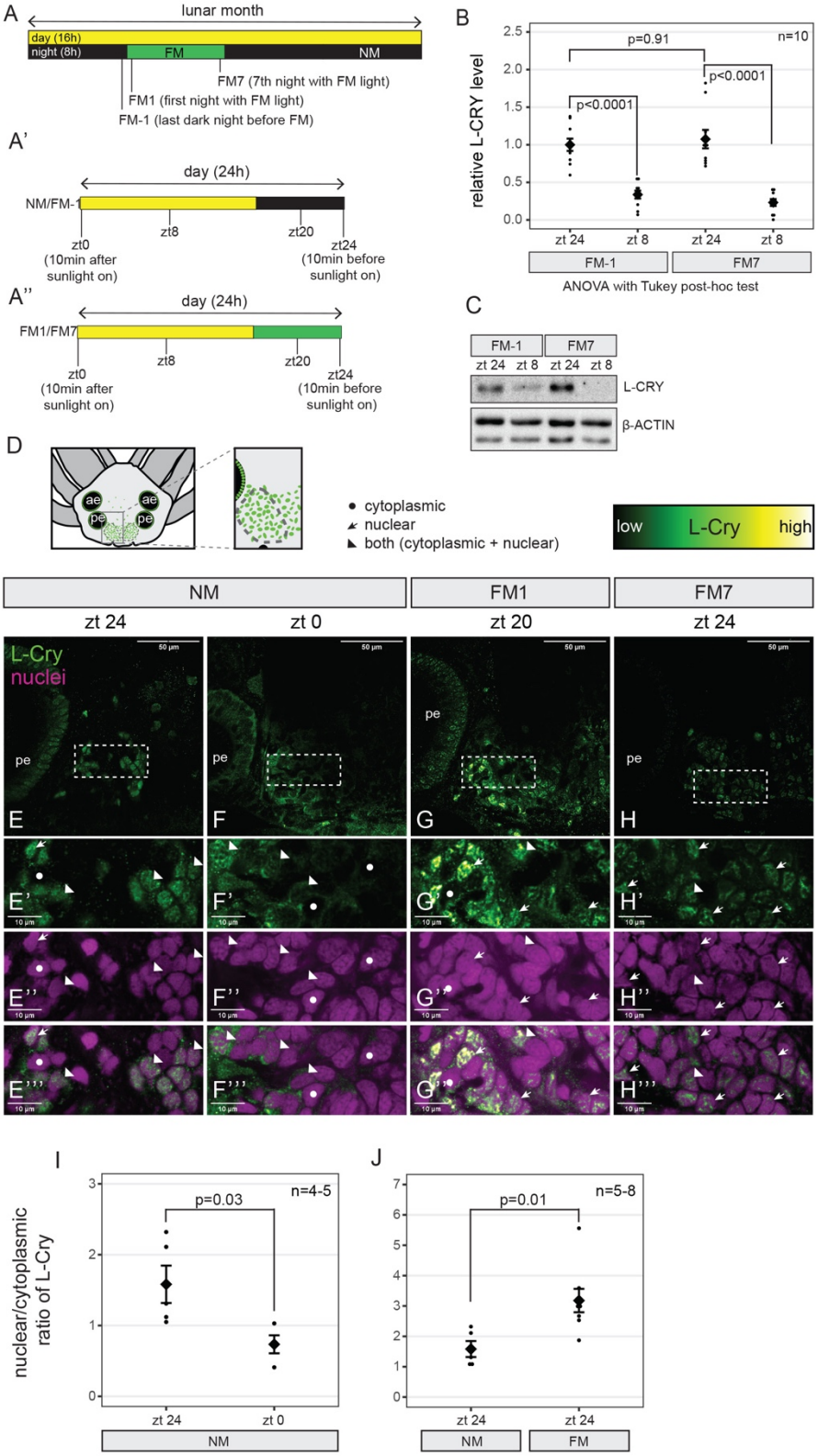

Figure 3: Naturalistic moon- and sunlight impact differently on L-Cry localization and levels.
(A,A',A'') Scheme of sampling timepoints. 16hrs day and 8 hrs night per 24hrs, 8 nights of moonlight per month. **(B)** relative L-Cry levels at indicated timepoints, as determined by Western Blot. Individual data points as well as mean ± SEM are shown. **(C)** Representative Western Blot used for quantification in (B), see fig.S9 for all other. **(D)** *P.dumerilii* head scheme. Dashed ovals designate the oval-shaped posterior domains between the posterior eyes. Green dots: L-Cry+ cells. ae, anterior eye; pe, posterior eye. **(E-H)** Maximal projections of confocal images of worm heads stained with anti-L-Cry antibody (green) and HOECHST (magenta: nuclei). White rectangles: areas of the zoom-ins presented below. zoomed pictures: single layers (1.28µm). Arrows: nuclear L-Cry, dots: cytoplasmatic L-Cry, arrowheads: both cytoplasmic and nuclear L-Cry. Overview images with nuclear stain: fig. S4 A-D. **(I,J)** quantification of subcellular localization of L-Cry as

nuclear/cytoplasmic ratio at indicated timepoints. Individual data points as well as mean ± SEM are shown. p-values: two-tailed t-test. For quantification as categorical data, see fig.S4E-G, S8.

In contrast to sunlight, exposure of L-Cry to 8h of naturalistic moonlight did not cause a reduction in L-Cry levels compared to an equivalent time in darkness (FM-1, zt24 versus FM7, zt 24: Figs.3B,C). Thus, any potential moonlight signalling via L-Cry occurs via a mechanism independent of L-Cry degradation.

We next examined the spatial regulation of L-Cry in worm heads (scheme Fig. 3D) at lunar and diel timepoints (Fig. 3A-A''). At NM, zt24, L-Cry is found predominantly in both nucleus and cytoplasm of individual cells, (Fig. 3E-E''', quantification as numerical data, i.e. nuclear/cytoplasmic ratio: Fig. 3I,J, for quantification as categorical data (*24*): fig.S4E-G). Already after 10mins of exposure to naturalistic sunlight (NM zt0, Fig. 3A,A'), the L-Cry nuclear localization strongly diminishes, becoming increasingly only cytoplasmic (Fig. 3F-F''', numerical quantification Fig. 3I, categorical quantification fig.S4E,F, also see accompanying manuscript Zurl et al). This suggests that naturalistic sunlight causes a shift of the protein to the cytoplasm, followed by degradation (FM-1, zt8, Fig. 3B,C, also see accompanying manuscript Zurl et al).

On the first night lit by the naturalistic moonlight for circalunar entrainment, L-Cry is strongly present at zt20, a timepoint which is consistent with having sufficient time to biochemically respond to naturalistic moonlight and to reach its moonlight-state (FM1, zt20, Fig. 3A,A'', G-G'''), thus fulfilling a prerequisite for moonlight sensation. Upon further naturalistic moonlight exposure for seven continuous nights (FM7, zt24) L-Cry remained clearly nuclear (Fig. 3H-H''', numerical quantification Fig. 3J, categorical quantification: fig.S4G). Thus, the sunlight and moonlight-states of L-Cry correlate with clearly distinct subcellular distribution patterns. In fact, we observed that L-Cry at FM7, zt24 is even more nuclear restricted than at zt24 under NM, both in the numerical analysis of the nuclear/cytoplasmic ratio (Fig. 3J), as well as in the blind categorical scoring (fig.S4G). This suggests that also the dark and moonlight states of L-Cry have distinct subcellular distribution patterns.

Taken together, these findings show that moonlight and sunlight impact differentially on L-Cry quantity and localization. The translocation of L-Cry from nucleus to cytoplasm in response to sunlight followed by reduced L-Cry levels suggests canonical degradation of L-cry in the cytoplasm. In contrast, moonlight does not cause L-Cry degradation, but might further shift its subcellular localization towards the nucleus.

L-cry mutants entrain less well than wildtype to naturalistic moonlight

As we found that L-Cry can respond to naturalistic moonlight biochemically, is present at night when moonlight can occur and responds differently to naturalistic moon vs. sunlight, we next wondered, if the circalunar clock responds differently to naturalistic moonlight in *Platynereis* wt versus *l-cry-/-* worms. We performed a circalunar re-entrainment experiment: animals initially raised and entrained

under “standard worm room light” conditions of artificial sun- and moonlight (fig. S3B,E) were challenged by a deviating FM stimulus of 8 nights of “naturalistic moonlight” (Fig. 4A, figs. S3C,E). This re-entraining stimulus was repeated for three consecutive months (Fig. 4A).

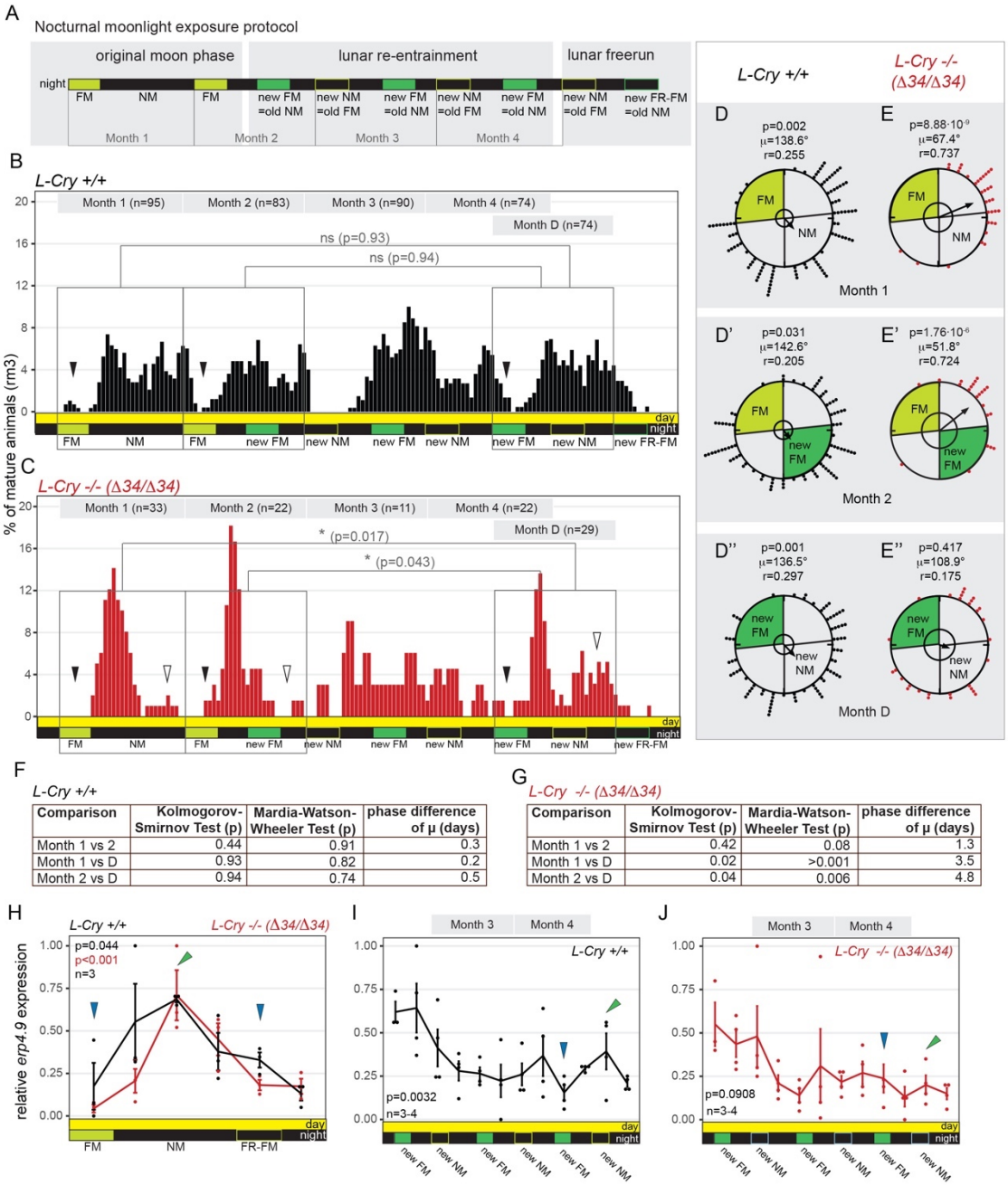

Comparison	Kolmogorov-Smirnov Test (p)	Mardia-Watson-Wheeler Test (p)	phase difference of μ (days)
Month 1 vs 2	0.44	0.91	0.3
Month 1 vs D	0.93	0.82	0.2
Month 2 vs D	0.94	0.74	0.5

Comparison	Kolmogorov-Smirnov Test (p)	Mardia-Watson-Wheeler Test (p)	phase difference of μ (days)
Month 1 vs 2	0.42	0.08	1.3
Month 1 vs D	0.02	>0.001	3.5
Month 2 vs D	0.04	0.006	4.8

Figure 4: *l-cry* contributes to circalunar clock entrainment
(A) Nocturnal moonlight exposure protocol of lunar phase shift with 8 nights of naturalistic moonlight. **(B,C)** Number of mature animals (percent per month, rolling mean with a window of 3 days) of *l-cry* wildtype (B) and mutant (C) animals. p-values: Kolomogorov-Smirnov tests. Black arrowheads indicate spawning-free intervals of the wildtype. White arrowheads in (C) designate the increasing second peak in the *l-cry* mutant after re-entrainment. **(D,E)** Data as in (B,C) plotted as circular data. 360° correspond to 30 days of the lunar month. The arrow represents the mean vector μ. r (length of μ) indicates phase coherence (measure of population synchrony). p-values are results of Rayleigh Tests: Significance indicates non-random distribution of data points. The inner circle represents the Rayleigh critical value (p=0.05). **(F,G)** Results of multisample statistics on spawning data shown in (A-E). **(H)** Circalunar regulation of *erp4.9* transcript levels in wildtype and mutant animals (heads of immature animals, lab condition, 6 nights of full moon). Individual data points as well as mean ± SEM are shown. p-values: one-way ANOVA. **(I,J)** Expression of the lunar regulated gene *erp4.9* in premature heads of wildtype (I) and *l-cry* mutants (J) during the lunar phase shift experiment. p-values: one-way ANOVA.

219 The resulting maturation peaks were analysed for the efficacy of this "naturalistic moonlight" to
220 phase-shift the circalunar oscillator. In order to judge how each population responded, we compared
221 the spawning distribution of the months before with the last month of the phase shift for each
222 genotype.
223 For an explanation of the noticeable difference in spawning distribution comparing identical months
224 between genotypes, see Fig. 5 and corresponding section below.

225 Under the re-entrainment regime (Fig. 4A), wildtype animals completely shifted their spawning
226 pattern, as supported by two statistical analyses:
227 (1) No significant difference in Kolmogorov-Smirnov test when comparing months 1 and 2 before the
228 shift to the newly entrained last month (month D) of the shift (Fig. 4B: grey rectangles, Fig. 4F);
229 (2) no significant difference in phase distribution with circular analyses of the same data when
230 comparing the months before the shift with the last month of the shift (Fig. 4D, D' versus D'', F).
231 Phase coherence (indicated as vector length r, a measure of population synchrony), was also very
232 similar before and in the last month of the shift r=0.255 and r=0.297) and the resulting phase
233 difference was 0.2 and 0.5 days, respectively (Fig. 4F).
234 In contrast, the spawning distribution of *l-cry* mutants shifted less than that of their wildtype
235 counterparts based on the same criteria:

236 (1) Kolmogorov-Smirnov testing showed significant differences in spawning distribution when
237 comparing months 1 and 2 before the shift to the last month of the shift (Fig. 4C: grey rectangles, Fig.
238 4G);

239 (2) a significant difference in the phase distribution in the circular analyses when comparing the
240 months before the shift with the last month of the shift (Fig. 4E,E' versus E'', G). The population also
241 exhibited a much lower phase coherence in the last month of the shift (r=0.175) than before the shift
242 (r=0.737), and a noticeable phase difference of 3.5 and 4.8 days, respectively (Fig. 4G).

243 Consistent with a less coherent shift of the *l-cry-/-* mutant population, we observed a pronounced
244 second peak in the last month of the phase shift, likely representing a subpopulation of worms that
245 still obeyed the old lunar phase (Fig. 4C, compare white arrowheads). A similar relative increase of
246 worms in the second part of the lunar months was not noticeable for the wildtype population (Fig.
247 4B).

248 In order to verify our phase shift results with an independent assay, we analyzed a molecular read-
249 out. We had previously identified *erp4.9* as being regulated by the circalunar clock on transcript and
250 protein level (*25*). qPCR analyses after long-term monthly entrainment validated *erp4.9* regulation
251 across the lunar month in both wildtype and mutant worms with identical phase and amplitude (Fig.
252 4H), and thus suitable for phase comparisons between wildtype and mutant worms in re-

253 entrainment analyses. We started the molecular analysis at the first new full moon and subsequently
254 sampled every week at zt6. Initially, both wildtype and mutants showed high expression (as expected
255 for the original NM phase), likely representing the situation that most worms were still entrained to
256 the original lunar phase (Fig. 4I,J). The levels of *erp4.9* for wildtype and mutants subsequently
257 lowered and remained low for several weeks, possibly representing populations of worms with
258 mixed circalunar phases (Fig. 4I,J). Importantly, during the third re-entrainment month, *erp4.9* levels
259 in wildtype animals indicated a shift of the circalunar clock, with low levels exactly matching the new
260 FM, and peak levels matching new NM (compare blue and green arrowheads black curve Fig. 4H vs.
261 I). By contrast, in the *l-cry -/-* population, such a profile was not detectable (compare blue and green
262 arrowheads red curve Fig. 4H vs. J).

263 Taken together, both spawning data and *erp4.9* expression dynamics suggest that *l-cry* mutant
264 populations entrain less well to naturalistic moonlight than wildtype, providing evidence that L-Cry is
265 part of the circalunar entrainment pathway.

266 *l-cry* mutants show altered lunar spawning synchrony

267 Another phenotype that is obvious from the above spawning data is that homozygous *l-cry*$^{-/-}$ animals
268 grown under conventional culture light conditions (i.e. artificial sun- and moonlight fig.S3B) showed a
269 higher population synchrony (r) than wildtype or heterozygous animals, exhibiting sharper spawning
270 peaks (Fig. 5A-C). This difference between mutants, wildtype and heterozygous animals is statistically
271 significant (Fig. 5A-C, Kolmogorov-Smirnov-Test on overall data distribution, Fig. 5I) and also well
272 visible in the circular analyses (Fig. 5E-G): Wildtype siblings and heterozygous worms distribute their
273 spawning across a lunar month significantly different from random (Rayleigh test $p=1.75x10^{10}$ and
274 $p=3.13x10^{8}$), but with rather low phase coherence, i.e. population synchrony (r=0.295 and r=0.222),
275 consistent with the wildtype data from the phase shift experiment (Fig. 4B,D-D''). In contrast,
276 homozygous *l-cry*$^{-/-}$ mutants exhibit a high phase coherence (r=0.614), consistent with the mutant
277 data from the phase shift experiment (Fig. 4C, E-E'). The differences between mutant and
278 wildtype/heterozygous controls are also highly significant by the Mardia-Watson-Wheeler test on the
279 circular data (Fig. 5I). The specificity of this phenotype of higher spawning precision for mutations in
280 the *l-cry* gene was confirmed by analyses on trans-heterozygous *l-cry* $^{(\Delta 34/\Delta 11)}$ mutants (fig. S5A-E), and
281 by the fact that such a phenotype is not detectable in any other light receptor mutant available in
282 *Platynereis* (*r-opsin1*: fig. S6A,B,E,F,I; *c-opsin1:* fig. S6C,D,G,H,I, *Go-opsin*: refs. (*26, 27*)).

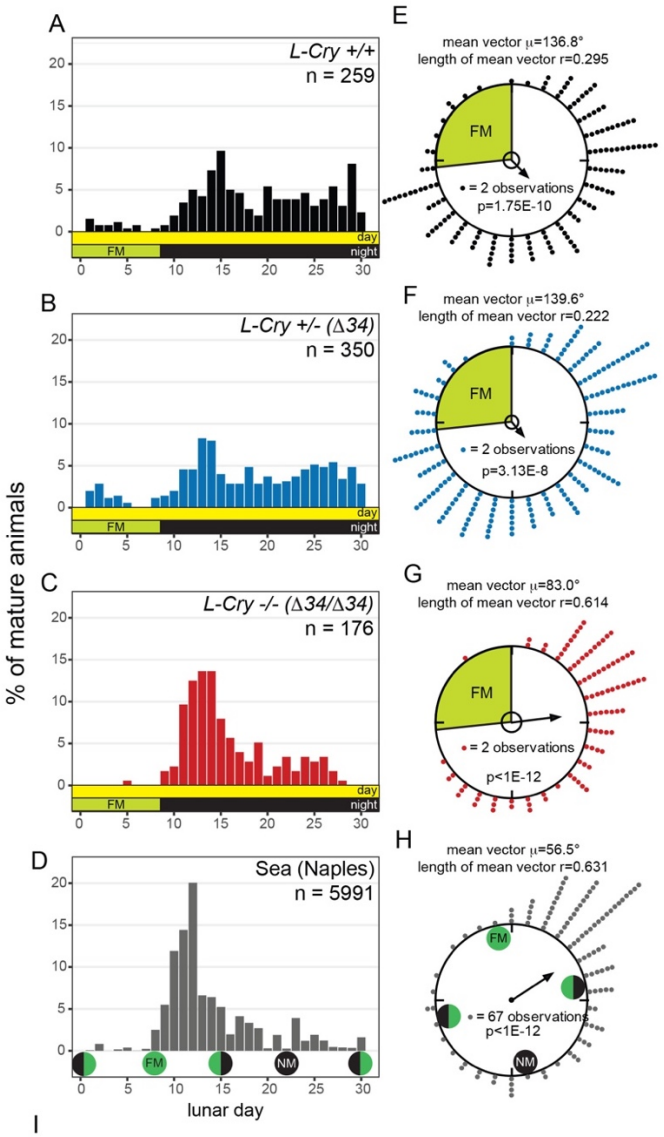

I

Comparison	Kolmogorov-Smirnov Test (p)	Mardia-Watson-Wheeler Test (p)	phase difference of μ (days)
L-Cry +/+ vs. *L-Cry* -/- wormroom light	$4.45 \cdot 10^{-7}$	$6.29 \cdot 10^{-7}$	4.5
L-Cry +/+ vs. *L-Cry* +/- wormroom light	0.142	0.155	0.2
L-Cry +/- vs. *L-Cry* -/- wormroom light	$2.43 \cdot 10^{-6}$	$2.46 \cdot 10^{-9}$	4.7
wt sea vs. *L-Cry* +/+ wormroom light	$< 2.2 \cdot 10^{-16}$	$<10^{-12}$	6.7
wt sea vs. *L-Cry* +/- wormroom light	$< 2.2 \cdot 10^{-16}$	$<10^{-12}$	6.9
wt sea vs. *L-Cry* -/- wormroom light	$3.04 \cdot 10^{-13}$	$5.08 \cdot 10^{-4}$	2.2

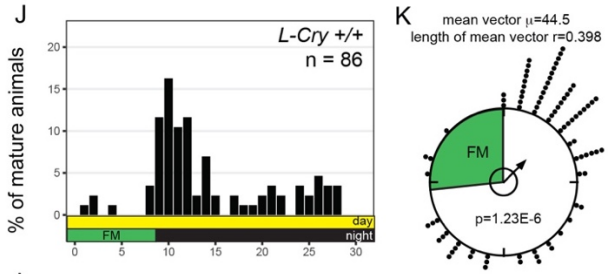

L

Comparison	Kolmogorov-Smirnov Test (p)	Mardia-Watson-Wheeler Test (p)	phase difference of μ (days)
L-Cry +/+ wormroom vs naturalistic light	$6.38 \cdot 10^{-10}$	$3.58 \cdot 10^{-8}$	7.7
wt sea vs *L-cry* +/+ naturalistic light	0.058	$5.99 \cdot 10^{-4}$	1.0

Figure 5: L-Cry shields the circalunar clock from light that is not moonlight
(A-D,J) Spawning of *l-cry* +/+ (A), *l-cry* +/- (Δ34) (B) and *l-cry* -/-(Δ34/ Δ34) (C) animals over the lunar month in the lab with 8 nights of moonlight (A-C), under natural conditions in the sea (D, replotted from ref. (*28, 29*)) and in the lab using naturalistic sun- and moonlight (J, 8 nights moonlight). **(E-H,K)** Data as in (A-D,J) as circular plot. 360° correspond to 30 days of the lunar month. The arrow represents the mean vector μ. r (length of μ) indicates phase coherence (measure of population synchrony). p-values inside the plots: Rayleigh Tests. Significance indicates non-random distribution of data points. The inner circle represents the Rayleigh critical value (p=0.05). **(I,L)** Results of multisample statistics on spawning data shown in (A-H,J-K).

We noticed, however, that the higher spawning synchrony in *l-cry*$^{-/-}$ worms mimics the actual spawning synchrony of *Platynereis dumerillii* populations in their natural habitat (Fig. 5D,H,I; r=0.631,

286 data from ref. (*28*)). Given that recent, non-inbred isolates from the same habitat as our lab inbred
287 strains exhibit a very similar (broad) spawning distribution under standard worm culture light
288 conditions (*30*), we reasoned that the difference in spawning synchrony between the normal
289 wildtype in culture versus at its natural habitat is caused by the rather crude light stimulus typically
290 used for the standard laboratory culture (fig. S3). The high population synchrony of *l-cry-/-* animals
291 that is close to natural conditions would suggest that L-Cry, as a molecular sun- vs. moonlight
292 discriminator, detects that the highly artificial nocturnal light is not proper moonlight and prevents it
293 from efficiently setting the worms' circalunar clock. This makes the predictions that an extended
294 exposure of the wild-type culture to our "naturalistic" moonlight should lead to a significant increase
295 of entrainment precision.
296 To test this hypothesis, we assessed the impact of adjusting light intensities and spectrum to
297 naturalistic sun- and moonlight (fig. S3C), maintaining the default temporal regime (8 nights of "full
298 moon"). Indeed, just adjusting light qualities indeed improved the precision and phase coherence of
299 population-wide reproduction: After several months under naturalistic sun- and moonlight, wildtype
300 worms spawned with a major peak highly comparable to the wildtype at the natural habitat (Fig.
301 5D,H vs. J,K), and also exhibited an increased population synchrony (r=0.398 compared to r=0.295
302 under standard worm room light conditions). This increased similarity to the spawning distribution at
303 the natural habitat ("Sea") is confirmed by statistical analyses (Fig. 5L), revealing a phase difference
304 of only 1 day, and no significant difference in the Kolmogorov-Smirnov test. In contrast, the spawning
305 distribution of wildtype under standard worm room light versus naturalistic light conditions is highly
306 significantly different in both tests and has a phase difference of 7.7 days (Fig. 5L).
307 These findings evidence that L-Cry blocks artificial, but not naturalistic moonlight from efficiently re-
308 setting the circalunar clock of wildtype animals. This block is removed in *l-cry-/-* animals, leading to a
309 better synchronization of the *l-cry-/-* population. This suggests that L-Cry's major role in circalunar
310 clock entrainment could be that of a signal gate-keeper.

311 *l-cry* functions as a light signal gate-keeper for circalunar clock
312 entrainment

313 A further prediction of this hypothesis is that in a re-entrainment regime using the highly artificial
314 (and not the naturalistic) moonlight, *l-cry-/-* mutants should entrain better than wild-type.
315 In fact, we had performed such a re-entrainment experiment early on during the analysis of the *l-cry-*
316 */-* mutants. (And were initially puzzled by its results.) We compared the spawning rhythms of *l-cry*$^{+/+}$
317 and *l-cry*$^{-/-}$ worms under a re-entrainment paradigm, where we provided our bright artificial culture
318 moon at the new moon phase (Fig.6A). Using these highly artificial nocturnal light conditions, the re-
319 entrainment of *l-cry*$^{-/-}$ animals was both faster and more complete than for their wildtype relatives.
320 This is evident from the linear data analysis and Kolmogorov-Smirnov tests when comparing the

321 month before the entrainment (month 1) with two months that should be shifted after the
322 entrainment (month D,E) (Fig. 6B,C,F,G). Most notably, while *l-cry-/-* worms are fully shifted in month
323 E, wildtype animals are mostly still spawning according to the initial lunar phase (boxes, blue
324 arrowheads Fig.6B,C). The faster re-entrainment of *l-cry*$^{-/-}$, compared to *l-cry+/+* animals is also
325 confirmed by the Mardia- Watson Wheeler test and the phase differences from the circular analysis
326 (Fig. 6D-G).

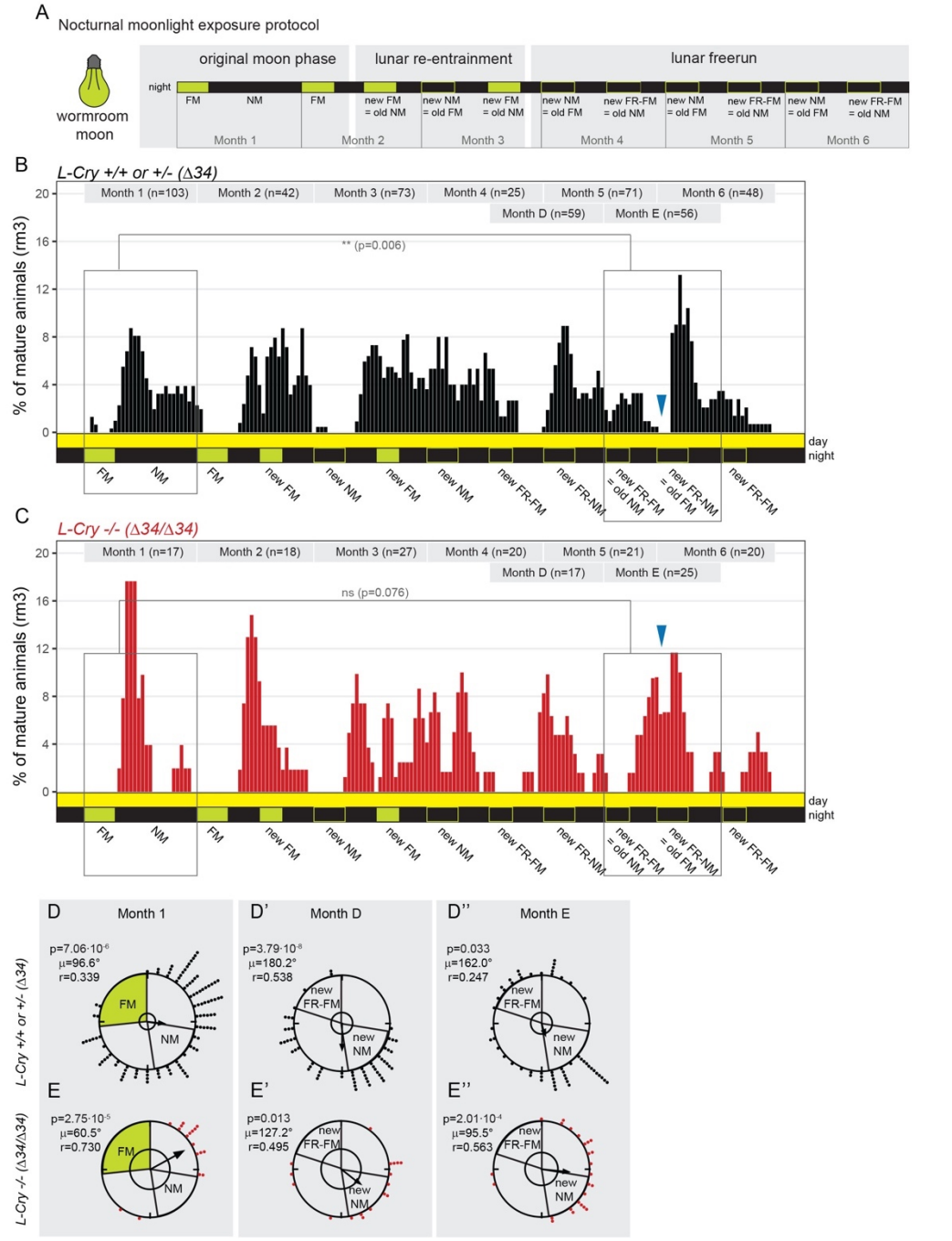

F *L-Cry +/+ or +/- (Δ34)*

Comparison	Kolmogorov-Smirnov Test (p)	Mardia-Watson-Wheeler Test (p)	phase difference of μ (days)
Month 1 vs D	$1.2 \cdot 10^{-6}$	$7.5 \cdot 10^{-6}$	7.0
Month 1 vs E	0.006	0.002	5.5

G *L-Cry -/- (Δ34/Δ34)*

Comparison	Kolmogorov-Smirnov Test (p)	Mardia-Watson-Wheeler Test (p)	phase difference of μ (days)
Month 1 vs D	0.002	0.002	5.6
Month 1 vs E	0.08	0.02	2.9

Figure 6: *l-cry-/-* mutants entrain the circalunar clock faster than wt to a high intensity artificial moonlight stimulus **(A)** Nocturnal moonlight exposure protocol of lunar phase shift (entrained by 8 nights, phased shifted by 6 nights of artificial culture moon). **(B,C)** Number of mature animals (percent per month, rolling mean with a window of 3 days) of *l-cry* wildtype (B) and homozygous mutant (C) animals. p-values indicate results of Kolomogorov-Smirnov tests. Blue arrowheads: spawning minima in wt versus mutant populations, respectively. **(D-E)** Circular plots of the data shown in (B) and (C). Each circle represents one lunar month. Each dot represents one mature worm. The arrow represents the mean vector μ. r (length of μ) indicates phase coherence (measure of population synchrony). The inner circle represents the Rayleigh critical value (p=0.05). **(F,G)** Results of multisample statistics of data in (D,E).

336 This provides further evidence that L-Cry normally blocks the "wrong" light from entering into the
337 circalunar clock and thus functions as a gate-keeper to optimize for the correct signal interpretation
338 in the highly complex natural light environment of the worms (Fig.7).

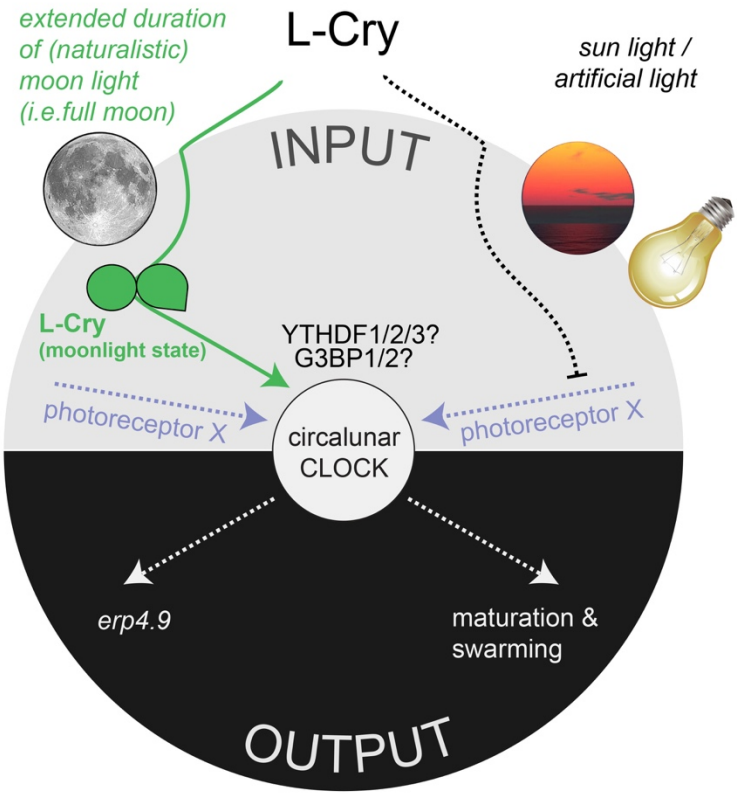

Figure 7. L-Cry functions as moonlight duration and valence detector for circalunar clock entrainment. L-Cry's biochemical property of only reaching the full moonlight state after extended periods of (naturalistic) moonlight illumination allow for a discrimination of moonlight duration. As moon phases are characterized by the duration of the moon on the night sky, moonlight exposure duration translates into moon phase detection. L-Cry also discriminate the valence of light, strongly favoring (naturalistic) moonlight to entrain the circalunar clock. YTHDF1/2/3 and G3BP1/2 are putative L-Cry interactors, possibly mediating part of the signal processes.

339

340 # L-Cry may functionally couple to two circalunarly regulated proteins
341

342 Finally, in order to next obtain a first understanding how L-Cry might link to the circalunar clock, we
343 employed a biochemical pull-down approach, coupled to mass spectrometry- based identification of
344 candidates.

345 Purified dark-adapted L-Cry was used as a bait to pull down proteins from wildtype worm head
346 extracts. We identified 11 putative interactors, two of which had been previously identified as
347 circalunarly regulated on protein level (*16*): a common ortholog of vertebrate Ras-GTPase binding
348 proteins 1 and 2 (hit 2: *Pdu*- G3BP1/2) and of vertebrate YTH domain containing factors 1, 2 and 3
349 (hit 5: *Pdu*- YTHDF1/2/3) (fig. S7A-C). As these interaction candidates could provide insight into the
350 circalunar entrainment pathway, we focused on them. First, we tested if the localization of *g3bp1/2*
351 and *ythdf1/2/3* mRNA overlaps with L-Cry positive cells, as a minimal requirement for a biologically
352 relevant interaction. (We tested the mRNA localisation of *g3bp1/2* and *ythdf1/2/3* as we at present
353 do not have antibodies against these proteins.) Indeed, *g3bp1/2* (Fig. 8A) and *ythdf1/2/3* (Fig. 8B)

354 showed an overlap in expression domains with *l*-cry (compare Fig. 2D) in the posterior oval-shaped
355 domain and the eyes. We next combined *in situ* hybridisation with L-Cry antibody staining. Indeed,
356 both *g3bp1/2* and *ythdf1/2/3* localize to L-Cry positive cells as indicated by the dark precipitate
357 surrounding an L-Cry+ nucleus (arrowheads pointing at examples in Fig. 8A',B'), supporting that they
358 are present in the same cells and can thus in principle function together with L-Cry.

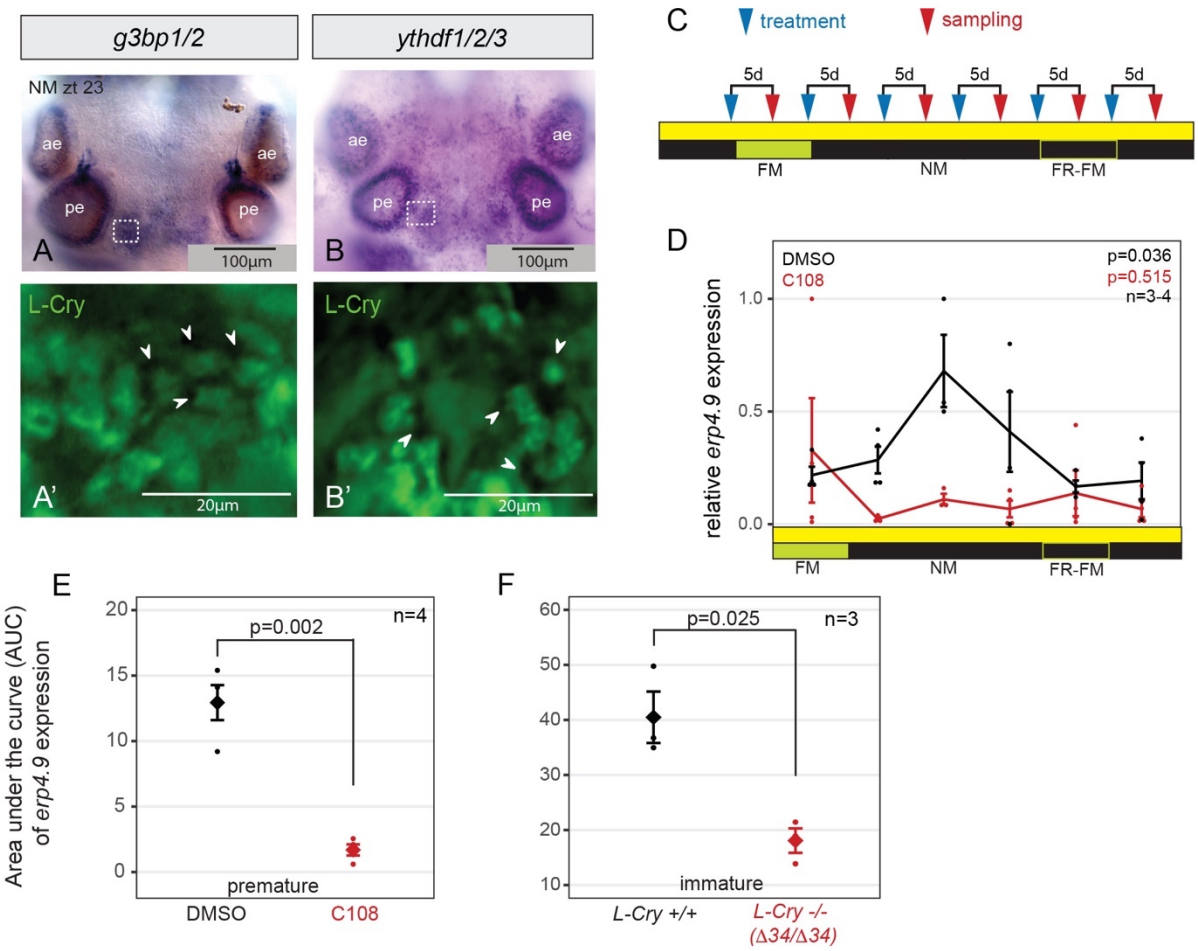

359

360 **Figure 8 : The putative L-Cry interactors G3BP1/2 and YTH1/2/3 are co-expressed with L-Cry and pharmacological**
361 **inhibition of G3BP1/2 affects the circalunar clock.**
362 **(A,B)** Whole-mount *in situ* hybridization (WMISH) in premature worm heads combined with L-Cry antibody staining (green).
363 Note that the purple precipitate of the WMISH signal is seen black on the fluorescent images. Arrowheads: cells with
364 cytoplasmic WMISH signal and nuclear L-Cry. Rectangles in (A) and (B) indicate region shown in (A',B'). ae, anterior eye; pe,
365 posterior eye. **(C)** Experimental scheme of C108 treatment. **(D)** Expression levels of *erp4.9* over the lunar month upon C108
366 treatment in heads of premature animals. p-values: one-way-ANOVA. **(E)** Area under the curve of *erp4.9* expression shown
367 in (D). **(F)** Area under the curve of *erp4.9* expression in immature worm heads calculated from the non-normalized data
368 from Fig.4H. p-values in (E) and (F) are results of t-tests. Individual data points as well as mean ± SEM are shown in (D-F).
369 Note that different stages of animals were used in (E) versus (F), impacting on absolute levels (*25*), but not relative
370 regulation.

371 If either of the two putative functional L-Cry partners is indeed involved in the circalunar mechanism,
372 interfering with them should have an effect on circalunar timing. We thus treated pre-mature worms
373 with the G3BP2 inhibitor C108 (*31*) throughout a circalunar month (scheme Fig.8C) and measured
374 *erp4.9* expression levels as a marker for circalunar clock phase (Fig. 4H). Upon a test of multiple
375 concentrations for short periods (data not shown), we decided to perform this multi-week

experiment with 10µM C108. This treatment caused *erp4.9* expression to no longer show significant changes in expression over the lunar month (Fig.8D) and furthermore reduced overall *erp4.9* expression levels (Fig. 8E). This indicated that *erp4.9* circalunar transcript rhythmicity is controlled by *Pdu*-G3BP1/2. In comparison, *g3bp1/2* expression levels were not affected by C108 treatment (fig. S7D,E), indicating that the effect on *erp4.9* is not caused by an overall effect on transcription. It is noteworthy that *erp4.9* levels were also significantly reduced in *l-cry-/-* worms (Fig. 8F). These data could indicate a possible involvement of G3BP1/2 in the L-Cry signalling of different light valences to the circalunar clock (Fig. 7).

Discussion

Our work delivers the first molecular entry point into the mechanisms underlying a moonlight-entrained monthly oscillator. It provides strong evidence that L-Cry is part of the lunar entrainment pathway and suggests a link to proteins that are themselves circalunarly regulated (Fig. 7). By this we advance the existing knowledge on Cryptochrome functions and non-circadian oscillators at multiple levels.

First, we provide biochemical evidence that at dim light levels, corresponding to moonlight in nature, L-Cry can accumulate photons over time. L-Cry's photoreduction response to this accumulation is in its duration markedly different from its rapid, well-established response to strong light and non-linear, suggesting that a different "moonlight" signalling state might exist. Second, consistent with different L-Cry states under dim and strong light, L-Cry under naturalistic moonlight is not following the conventional cytoplasmic degradation pathway, but localizes at higher levels to the nucleus. This suggests that different cellular compartments convey the different light messages to different downstream pathways. The regulation of the subcellular localization depending on light regime prompted us to look for any conventional nuclear localization sequences, which we could not detect in L-Cry.

Upon exposure to naturalistic daylight, L-Cry rapidly moves to the cytoplasm, where its protein levels become reduced, fully consistent with our previous data in S2 cells (*14*). In *Drosophila melanogaster* dCry is degraded via its light-induced interaction with the circadian clock protein Timeless and subsequent JETLAG (JET) ubiquitin-ligase–mediated proteolytic degradation (*32*). Given that both Timeless and Jetlag exist in *Platynereis* (*Pdu*-Tim: (*14*), *Pdu*-Jet: reciprocal best blast hit in ESTs), it is possible that a similar mechanism exists in *Platynereis*. It is however noteworthy that *timeless* transcript levels are regulated by room light in the bristle worm (*14*), indicative of additional levels of regulatory complexity.

409 In contrast to the suggested mechanism about L-Cry's fate in the cytoplasm based on existing
410 knowledge from its *Drosophila* ortholog, the signalling downstream of nuclear L-Cry is at present
411 completely enigmatic. It is clear from our data (and the accompanying manuscript Zurl et al) that
412 neither darkness nor naturalistic moonlight causes degradation of nuclear L-Cry. This might indicate
413 that ratios of cytoplasmic versus nuclear L-Cry could be important for circalunar clock moonlight
414 entrainment. To complicate matters even further- it is possible that different spatial expression
415 domains, such as eye versus brain, need to be considered separately in their responses to extended
416 naturalistic moonlight and subsequent downstream signalling cascades.

417 Without at present being able to provide spatial resolution, we offer a first glimpse at possible
418 downstream players, the proteins G3BP1/2 and YTHDF1/2/3. The localization of the mRNA of both
419 factors to L-Cry positive cells at least allows for a function of these proteins together in the same
420 cells. However, it is absolutely clear that follow-up studies with antibodies against both proteins will
421 be required to further verify and understand their interactions with L-Cry, and their possible
422 connection to the circalunar clock. The fact that a treatment of worms with the G3BP2 inhibitor C108
423 results in a disruption of the circalunar oscillations of *erp4.9* provides support for placing it in a
424 pathway with L-Cry and opens the question about possible functions in connection with the
425 circalunar clock. Interestingly, a common feature of the orthologs of both G3BP1/2 and YTHDF1/2/3
426 are their function in RNA-binding and regulation(*33-35*). Furthermore, a screen for interacting
427 proteins of YTHDF1, 2 and 3 in mammalian cells revealed G3BP1 and 2 among the top 25 interacting
428 proteins for each YTHDF(*35*), suggesting that these proteins can function within a complex. In the
429 perspective of possible roles in mRNA translation and stability this could provide an explanation for
430 our previous observation that changes on protein rather than transcript level are prominent between
431 the NM and FR-FM phase of the worm's circalunar clock (*25*), an observation that had already
432 prompted us to speculate about post-transcriptional processes being of high importance to the
433 functionality of the circalunar oscillator. But how does this connect with the localization of L-Cry to
434 the nucleus under darkness and - even more- under moonlight? Could it be possible that moonlight
435 removes remaining L-Cry from G3BP1/2 and YTHDF1/2/3 containing complexes in the cytoplasm and
436 by this impacts on the regulation of mRNA translation and stability? Is the observation that more
437 cells possess only nuclear L-Cry after 7 nights of naturalistic full moon compared with more nuclear
438 and cytoplasmic L-Cry under dark NM nights potentially relevant in this context? To further
439 complicate matters- it is in our opinion highly likely that L-Cry also has a function in the nucleus itself.
440 This could be independent of G3BP1/2 and YTHDF1/2/3, like transcriptional regulation. This has been
441 shown to occur for its ortholog in *Drosophila* (*36*). However, also G3BP1/2 and YTHDF1/2/3 orthologs
442 can be present in the nucleus (*33, 37*), and G3BP1/2 possesses a highly conserved NTF2-like domain.
443 The NTF2-like domain is structurally and functionally similar to NTF2 , which regulates nuclear

transport (*38*). It is thus also possible that the putative interaction between G3BP1/2 and L-Cry is involved in the cytoplasmic/nuclear shuttling of L-Cry and/or nuclear functions.

Connected to the question of the transmission of the moonlight signal to the circalunar oscillator is also a better understanding of L-Cry's "moonlight state". Is this state "just" a partial photoreduction of the state reached upon artificial sunlight exposure or perhaps also a conformationally different state with distinct formation and decay kinetics? And what is the role of the L-Cry dimers? An intriguing observation is, that in presence of moonlight the moonlight state can be stably maintained over several hours, whereas the sunlight state completely reverts to the fully-oxidized dark-state within minutes without accumulating the moonlight state while transitioning through partial photoreduction (Fig.1J). These different responses to moonlight illumination suggest that the moonlight- and sunlight states are conformationally and kinetically not equivalent (fig. S2I). Based on its sequence homology and the similarity of its FAD photoreaction to *Drosophila* CRY (dCry), it is conceivable that L-Cry also displaces the regulatory C-terminal tail in the photoreduced state as observed for dCry (*21*),(*39*). However, as dCry is monomeric, L-Cry homodimer formation may impact these conformational changes, and these may further vary depending on whether moonlight or sunlight operates on the initial dark-state L-Cry homodimer. We propose, that partial FAD photoreduction in the moonlight state could be related to the formation of asymmetric L-Cry dimers, where one monomer retains oxidized FAD, while in the second monomer FAD is photoreduced to $FAD^{\circ-}$ (Fig. 1J). This requires, that the flavins in the two L-Cry monomers have different redox potentials, likely resulting from different chemical environments due to conformational differences between the monomers (Fig. S2I). Hence different amounts of energy (photon numbers) would be needed to photoreduce the flavins in the two L-CRY monomers. Moonlight, due to its very low intensity can only induce the lower energy transition, resulting in the partially photoreduced moonlight state. In presence of intense sunlight, however, the larger energy barrier to photoreduce the second flavin can also be overcome. Certainly, more extensive mechanistic studies are required to further support our model. However, this model is consistent with all our current *in vitro* data, and moreover, it plausibly illustrates how the very different intensities of moon- and sunlight can lead to the formation of conformationally distinct dark state (new moon), moonlight state (full moon) and sunlight state L-Cry proteins. Thereby L-Cry could translate different light qualities into different cellular signaling events, e.g. by changing L-Cry's subcellular localizations and cellular degradation rates (Fig. 3), to ultimately affect moonlight dependent physiology (Fig. 4-7).

Finally, an evolutionary consideration: Monthly synchronization by the moon has been documented for a wide range of organisms- including brown and green algae, corals, crustaceans, worms, but also vertebrates (reviewed in (*6*)). Furthermore, recent reports also provide increasing evidence that the

lunar cycle influences human behaviour (reviewed in (*40, 41*)). Are the lunar effects mediated by conserved or different mechanisms? It is important to take the period lengths into consideration. In other words- just because an oscillation is controlled by the moon, doesn't mean it has the same mechanism. There is a big difference between a period length in the range of hours, versus a period length in the range of weeks. Thus, also for evolutionary comparisons, tidal and circalunidian/circadian rhythms should be considered differently from monthly rhythms (also see accompanying manuscript Zurl et al.).

When considering monthly oscillators with period lengths in the range of weeks, our implication of L-Cry as a light receptor in the circalunar entrainment pathway at first glance rather suggests that such monthly oscillator might not be conserved, given that direct L-Cry orthologs are not present in all the groups that are affected by the lunar cycle (*42*). However, taking further aspects into account, such a conclusion might be too quick. Could other members of the Cry/photolyase family take over similar functions? Could it also be that other cues, such as changes in the earth magnetic field provide additional entrainment cues? Furthermore, our entrainment data suggest the presence of additional moonlight photoreceptors.

Last, but not least the molecular mechanisms underlying the circalunar oscillator also await identification, and it is possible that conservation exists on this level. Examples are known from circadian biology and it will now require further work to reach a similar level of understanding for moon-controlled monthly rhythms and clocks.

Materials and Methods

Natural light measurements

Under water measurements of natural light at the habitat of *Platynereis dumerilii* were acquired using a RAMSES-ACC-VIS hyperspectral radiometer (TriOS GmbH) for UV to IR spectral range. In coastal waters of the Island of Ischia, in the Gulf of Naples, the two radiometers were placed on sand flat at 5m depth near to *Posidonia oceanica* meadows, which are a natural habitat for *P. dumerilii.* Measurements were recorded automatically every 15min across several weeks in the winter 2011/2012. To obtain a fullmoon spectrum, measurements taken from 10pm to 1am on a clear fullmoon night on the 10.11.2011 were averaged. To subtract baseline noise from this measurement, a NM spectrum was obtained by averaging measurements between 7:15pm to 5am on a NM night on 24.11.2011, and subtracted from the FM spectrum. Resulting spectrum: fig. S3A. To benchmark these moonlight spectra measured under water with moonlight measured on land, we compared the underwater spectra to a publicly available full moon spectrum measured on land on 14.04.2014 in the Netherlands (fig. S3G, spectrum available at http://www.olino.org/blog/us/articles/2015/10/05/spectrum-of-moon-light). As expected, light with

512 longer wavelengths was strongly reduced in the underwater measurements compared to the surface
513 spectrum, since longer wavelengths penetrate water less efficiently. For the sunlight spectrum,
514 measurements taken from 8am to 4pm on a sunny day on 9.11.2011 were averaged.

515 Naturalistic Light Systems (NELIS devices)

516 To emulate naturalistic sunlight and moonlight conditions, we employed NELIS (Natural Environment
517 Light Intensity System) (Marine Breeding Systems GmbH)(*22*). The naturalistic moonlight device was
518 composed of a combination of LEDs and an Ulbricht sphere for homogenous light mixing. For
519 improved light distribution across the shelf, a naturalistic moonlight device was attached to each end
520 of an acrylglass rod (two light sources and one rod per shelf). For details on the naturalistic sunlight
521 source see ref. (*22*). Light spectra were measured using ILT950 Spectroradiometer (International
522 Light Technologies).

523 Cloning and recombinant virus generation for L-Cry

524 Full length N-terminally His_6-tagged *Platynereis dumerilii* L-Cry (1-567) was heterologously expressed
525 in *Spodoptera frugiperda (Sf9)* insect cells using the Bac-to-Bac baculovirus expression system with
526 the pCoofy27 expression vector. $1 * 10^6$ *Sf9* cells were transfected with recombinant bacmid DNA
527 using Cellfectin. The first generation P0 virus was harvested 3 days after bacmid transfection. A
528 further virus amplification step was carried out and the P1 virus stock was used for protein
529 expression. The volume of P1 virus stock to be added for sufficient protein expression was
530 determined by test expression.

531 Protein expression and purification

532 *Sf9* cells were grown as suspension cultures in sf900II media at 27°C, 80 RPM. 1 L of $1 * 10^6$ *Sf9*
533 cells/ml were transfected with P1 virus stock and incubated at 27°C for 72 h. Cells were harvested by
534 centrifugation at 7000 rpm for 20 min and stored at -80°C until purification. All purification steps
535 were carried out in dark or dim red light conditions. Columns were wrapped with aluminum foil to
536 avoid light-activation of L-Cry. The cell pellets were resuspended in lysis buffer (20 mM Tris pH 7.5,
537 150 mM NaCl, 20 mM imidazole, 5% glycerol, 5 mM β-mercaptoethanol) and lysed using a
538 microfluidizer. The lysate was centrifuged at 27000 rpm for 45 min and the clarified supernatant
539 incubated with nickel beads for 1 h. The nickel beads were loaded onto a batch column, washed with
540 50-100 mM imidazol and the L-Cry protein was eluted with 250 mM imidazole. Elution fractions
541 containing L-Cry were concentrated, diluted with low salt buffer (50 mM Tris pH 7.5, 50 mM NaCl, 5%
542 glycerol, 1mM DTT) and loaded onto a 5 ml Hitrap Q sepharose anion exchange column (GE
543 Healthcare). A gradient from 0 % to 100 % high salt buffer (50 mM Tris pH 7.5, 1 M NaCl, 5% glycerol,
544 1mM DTT) was applied. L-Cry containing fractions were pooled, concentrated and loaded onto a
545 HiLoad S200 16/60 size exclusion chromatography (SEC) column (buffer 25 mM Bis-Tris propane pH

546 8.0, 150 mM NaCl, 5% glycerol, 1 mM TCEP). Fractions containing pure L-Cry were pooled,
547 concentrated to 10 mg/ml and snap frozen in liquid nitrogen for storage at -80°C. 2 mg of L-Cry was
548 obtained from 10 g of pellet. The identity of the L-Cry protein was confirmed by mass spectrometry.

549 **Reverse-phase HPLC analyses of the chromophore content of L-Cry**

550 Flavin Mononucleotide (FMN), Flavin Adenine Dinucleotide (FAD) and Methenyltetrahydrofolate
551 (MTHF) were dissolved in buffer (25 mM Bis-Tris propane pH 8.0, 150 mM NaCl, 5% glycerol) and run
552 at 1ml/min (20 °C) over a Macherey-Nagel C18 Gravity-SB (150/4/5 µm) column to separate the
553 chromophores by reverse phase (RP) HPLC analyses. A gradient from 20-100% of methanol against
554 water (+0.1% Trifluoroacetic acid) was used for optimal separation. To analyse the chromophore
555 content of L-Cry, purified L-Cry was heat-denatured for 5 min at 97°C and centrifuged at 14000 RPM
556 for 10 min at 4°C. The supernatant was subjected to RP-HPLC analysis. The chromophores were
557 monitored by absorption at 370 nm.

558 **Analytical Size Exclusion Chromatography (SEC) and SEC coupled with Multiangle**
559 **light scattering (SEC-MALS)**

560 Analytical SEC of dark-state L-Cry was carried out on a S200 10/300 size exclusion column (SEC buffer
561 25 mM Bis-Tris propane pH 8.0, 150 mM NaCl) under red light conditions. SEC-MALS was carried out
562 to determine the exact molecular weight and oligomeric state of purified L-Cry based on the SEC
563 elution volume and light scattering. For SEC-MALS, purified L-Cry was loaded onto a Superose 6
564 10/300 size exclusion column and run at a flowrate of 0.4 ml/min in SEC buffer. MALS data were
565 obtained from a DAWN DSP instrument (Wyatt Tech, Germany) and processed using ASTRA 4.90.07.
566 Elution volumes and corresponding molecular weight of calibration standards: 10.3 ml – 670 kDa
567 (Thyroglobulin), 13.67 ml – 158 kDa (γ-globulin), 15.71 ml – 44 kDa (ovalbumin), 17.42 ml – 17 kDa
568 (myoglobin) and 20.11 ml – 1350 Da (vitamin B12).

569 **UV/VIS spectroscopy on L-Cry: Blue light-, sunlight- and moonlight photoreduction**
570 **and dark recovery**

571 UV/Visible absorption spectra of the purified L-Cry protein were recorded on a Tecan Spark 20M
572 plate reader unless otherwise stated. A light-state spectrum of L-Cry with fully photoreduced $FAD^{\circ-}$
573 was collected after illuminating dark-adapted L-Cry for 110 sec with a 450 nm blue light emitting
574 diode (fig S3D,E; 6.21 x 10^{16} photons/cm^2/sec at the sample). To analyze sunlight- and moonlight
575 dependent FAD photoreduction, dark-adapted L-Cry (kept on ice) was continuously illuminated with
576 naturalistic sunlight (fig. S3C,E; 1.55 x 10^{15} photons/cm^2/sec at the sample) or naturalistic moonlight
577 (fig. S3C,E; 9.65 x 10^{10} photons/cm^2/sec at the sample) and UV-VIS spectra (300 – 700 nm) were
578 collected at different time points.

579 Dark recovery kinetics (FAD reoxidation) of L-Cry at 18°C following illumination with blue-light (110
580 sec), sunlight (20 min on ice) or moonlight (6 h on ice) were measured by recording absorbance
581 changes at 450 nm over time or by extracting 450 nm absorbance values from complete UV/VIS
582 spectra. To measure dark recovery kinetics on ice, complete UV-VIS spectra (300 – 700 nm) were
583 collected at different time points following 110 sec blue light- or 20 min sunlight illumination and
584 absorbance values at 450 nm were extracted from the full spectra (sample was kept on ice and in
585 darkness between measurements). Additionally, a temperature controlled Jasco V-550 UV-VIS
586 spectrophotometer was used to determine dark recovery kinetics of L-Cry (after 110 sec blue-light) at
587 6°C based on absorbance changes at 450 nm. The time constants for dark recovery were calculated
588 by fitting a single exponential curve to the experimental data. Spectra were analyzed using Origin
589 (Version 7.5/10.5(trial); OriginLab Corporation, Northampton, MA, USA).

590 **Recovery of L-Cry dark state in presence of moonlight**

591 To assess if moonlight can maintain the light state, L-Cry was initially illuminated with sunlight for 20
592 min or with blue light for 110 sec, followed by continuous moonlight illumination up to 6 hours with
593 the sample kept on ice. Complete UV-VIS spectra (300 – 700 nm) were collected at different time
594 points. Absorbance values at 450 nm were taken from the complete spectra obtained between 5 min
595 and 2h 30 min moonlight exposure and used to determine the time constant for recovery of oxidized
596 FAD after blue-light or sunlight induced photoreduction in presence of moonlight.

597 **Sunlight illumination of moonlight activated L-Cry**

598 To assess if sunlight can further increase FAD photoreduction starting from the moonlight activated
599 state, L-CRY was first illuminated with continuous moonlight for 6 hours, followed by 20 min of
600 sunlight illumination (on ice). Complete UV-VIS spectra from 300 – 700 nm were measured in each
601 case.

602 **Pull-down of L-Cry interactors and mass spectrometry**

603 Pre-purified L-Cry with N-terminal His_6 tag was bound to magnetic nickel beads. 20 frozen worm
604 heads (ZT20) from new moon phase were resuspended in buffer (50mM Tris pH 7.5, 150 mM NaCl,
605 2.5 mM $MgCl_2$, 1% Triton X, 1mM phenylmethylsulfonyl fluoride, benzonase and cOmplete^{TM} EDTA-
606 free protease inhibitor cocktail tablets) and lysed by sonication. The tubes were wrapped with
607 aluminum foil and the pull-down experiment was done under red light. L-Cry bound to magnetic
608 nickel beads was used as bait (sample) and empty nickel beads as control. The worm head lysate was
609 incubated with magnetic nickel beads (sample and control) for 3 h at 4°C on rotation. The beads were
610 washed thrice with resuspension buffer (without 1% Triton X) and finally eluted with Lithium Dodecyl
611 Sulfate (LDS) buffer at 70°C for 10 min. The samples were loaded on NuPAGE 4-12% Bis-Tris
612 commercial gels, excised and prepared for in-gel digestion and dimethyl labelling. The experiment

613 was done in 2 replicates. Each sample and control elution was then used for labelling the digested
614 peptides with a heavy and light label (forward experiment) and with switching the label (reverse
615 experiment). The light and heavy labelling provided a list of interactors specifically enriched with L-
616 Cry as bait as compared to the control. The digested and purified peptides were later analyzed by
617 mass spectrometry. Q Exactive Plus mass spectrometer (Thermo Scientific) was used for all mass
618 spectrometry experiments. Stable-isotope dimethyl labeling was used for quantitative proteomics.
619 The MaxQuant software package (Version 1.5.2.8) was used for data analysis (*43-45*) with the
620 Uniport database Platynereis_dumerilli_(CLAMWORM)_Uniport_20190116.fasta and the in-house
621 generated worm head database Pdu_HeadRef_Prot_v4.fasta (*25*). Data analysis was done by
622 MaxQuant (Version 1.5.2.8) with default settings, except re-quantify was activated against an in-
623 house generated worm head database Pdu_HeadRef_Prot_v4.fasta. The output was further filtered
624 by removing known contaminants, reverse data base binders and proteins only identified by site
625 modification. We also filtered for minimum 2 peptides (minimum 1 unique) per protein group.

626 Worm Culture

627 *Platynereis dumerilii* were grown as previously described (*14, 46*). All animal work was conducted
628 according to Austrian and European guidelines for animal research. Photoperiod 16:8 (L/D),
629 circalunar entrainment: nocturnal light for 6-8 nights (see Figure legends for each experiment) every
630 29 to 30 days (centering around full moon ("inphase") or new moon ("outphase") in Vienna). Light
631 spectra and intensities of fig. S3 were measured with a recently calibrated ILT950 spectrometer
632 (International Light Technologies Inc Peabody, USA) and converted to photons/cm^2/s.

633 Generation and Genotyping of *l-cry* KO worms

634 Design and construction of TALENs targeting *l-cry* is described in (*23*). For genotyping, DNA extraction
635 of immature and premature worms was conducted by cutting 5-10 tail segments with a scalpel and
636 incubating them in 20µl 50mM NaOH at 95° for 20min. After adding 5µl of Tris/HCl pH 7.5, the
637 supernatant was used as template for the PCR reaction. Mature worms were frozen as whole at -
638 20°C and DNA was later extracted using NucleoSpin Tissue Mini kit for DNA from cells and tissue
639 (Macherey-Nagel). PCR was performed with OneTaq Quick-Load 2x Master Mix with Standard Buffer
640 (New England Biolabs). PCR product was run on an agarose gel and genotype was determined on size
641 (168bp: wildtype, 134bp: Δ34+Δ9 mutant allele, 157bp: Δ11 mutant allele).

Primer	**Sequence 5'-3'**
l-cry_fwd	AAGAGAAGACTGACGATTGGGAC
l-cry_rev	CTGCAACTTCCCCATCCC

642 *Primers used for l-cry genotyping*

643 Full length *l-cry* cDNA- GenBank: MW161054

644 **Monoclonal Antibody Production**

645 A peptide consisting of amino acids 52 - 290 of L-Cry protein (GenBank ID: MT656570, predicted size
646 25kDa) was cloned and expressed in bacteria cells. Subsequently, this peptide was purified and used
647 for mouse immunization, thereby acting as epitope in production of a monoclonal antibody against L-
648 Cry. Upon screening of multiple clones, two clones (4D4-3E12-E7 and 5E3-3E6-E8) were selected and
649 used in combination. Monoclonal antibodies were produced by and purchased from the Monoclonal
650 Antibody Facility at Max Perutz Labs (Medical University of Vienna, Department of Medical
651 Biochemistry).

652 **Immunohistochemistry, microscopy and L-Cry localization determination**

653 Worm heads were dissected with jaws and fixed in 4% PFA for 24h at 4°C. Samples were
654 subsequently permeabilized using methanol, digested for 5 min with Proteinase K at room
655 temperature without shaking and post-fixed with 4% PFA for 20 min at room temperature. Next,
656 samples were washed 5 times for 5 min with 1x PTW and incubated in hybridization mixture(*47*) used
657 in *in situ* hybridization protocol, at 65° C overnight. Worm heads were washed with 50%
658 formamide/2X SSCT - standard saline citrate containing 0.1% Tween 20® (Sigma Aldrich) (2x, 20 min),
659 then with 2X SSCT (2x, 10 min) and with 0.2X SSCT (2x, 20 min); all washing steps at 65° C. After
660 blocking for 90 min with 5% sheep serum (Sigma-Aldrich) at room temperature, samples were
661 incubated in L-Cry antibodies 5E3-3E6-E8 (1:100) and 4D4-3E12-E7 (1:50) in 5% sheep serum (Sigma-
662 Aldrich). Secondary antibody, Cy3 goat anti-mouse IgG (A10521, Thermo Fisher Scientific) was diluted
663 1:400 in 2.5% sheep serum (Sigma-Aldrich). Incubations were done for at least 36h at 4° C shaking
664 and after each incubation time, samples were washed with 1x PTW three times for 15 min at room
665 temperature and a fourth time over night at 4° C. After this, Höchst 33342 (H3570, Thermo Fisher
666 Scientific), diluted 1:2000, was added for at least 30 min at room temperature. Samples were then
667 washed three times for 15 min with 1x PTW at room temperature and mounted with 25 mg/ml
668 DABCO (Roth/Lactan) in an 87% glycerol (Sigma-Aldrich) solution. All solutions were made with 1x
669 PTW (PBS + 0.1% Tween 20®) (Sigma Aldrich). Heads were imaged on a Zeiss LSM 700 laser scanning
670 confocal microscope using LD LCI Plan-Apochromat 25X, Plan-Apochromat 40X by CHD: T-PMT
671 detection system and Zeiss ZEN 2012 software. Lasers: DAPI 405 nm and Cy3 555 nm.

672 Categorical scoring: Using Fiji/ImageJ (*48*), nuclear outlines were marked as Regions Of Interest (ROI)
673 on the 405 nm channel images (Höchst staining). ROIs were then used for scoring of the signal
674 localization (inside =nucleus versus outside= cytoplasm) on the 555nm channel of the same images
675 (L-Cry).

676 Quantitative scoring: Using the deep learning-based image segmentation algorithm Cellpose (*49*) on
677 the 405 nm channel images, the Hoechst-stained nuclei were identified and marked as Regions Of

678 Interest (ROI). L-Cry signal was then determined for these nuclear ROIs using in Fiji/ImageJ (*48*).
679 Signal intensity was determined by calculating Corrected Total Cell Fluorescence (CTCF) using the
680 formula CTCF=Area (ROI_1)*Mean (ROI_1)-Area (ROI_1)*Mean(ROI_(background ROIs)). A sum of
681 CTCF values of all the nuclei was subtracted from the CTCF value of the whole brain area, to obtain
682 the corresponding value for non-nuclear, i.e. cytoplasmic signal. Finally, the ratio between nuclear
683 and non-nuclear (cytoplasmic) signal intensity was calculated for corresponding regions of different
684 worm heads to compare between different ZTs.

685 **Protein extraction and Western Blots**

686 Per biological replicate four premature worms were anaesthetized (7.5% $MgCl_2$-/H_20, 1:1 diluted with
687 sea water), decapitated and heads transferred to a 1.5ml tube containing 150 µl RIPA lysis buffer
688 (R0278 Sigma-Aldrich), 10% Triton X100 and protease inhibitor (cOmplete Tablets, EDTA-free,
689 *EASYpack*, Roche). The tissue was homogenized by grinding using a tight fitting pestle. All steps on
690 ice. Cell debris was pelleted by centrifugation. Protein concentration of lysates was determined using
691 Bradford reagent (BIORAD), subjected to SDS-gel electrophoresis (10% Acrylamide) and transferred
692 (Transferbuffer: 39mM Gylcine, 48mM Tris, 0.04% SDS, 20% MetOH) to a nitrocellulose membrane
693 (Amersham™ Protran™ 0,45µm NC, GE Healthcare Lifescience). Quality of transfer was checked by
694 Ponceau-S (Sigma Aldrich) staining. After 1h of blocking with 5% slim milk powder (Fixmilch Instant,
695 Maresi) in 1xPTW (1xPBS/0.1% TWEEN 20) at room temperature, the membrane was incubated with
696 the appropriate primary antibody diluted in 2.5% milk/PTW at 4°C overnight. [anti-L-Cry 5E3-3E6-E8
697 (1:100) and anti-L-Cry 4D4-3E12-E7 (1:100); anti-beta-Actin (Sigma, A-2066, 1: 20.000)]. After 3 rinses
698 with 1xPTW the membrane was incubated with the species specific secondary antibody [anti-Mouse
699 IgG-Peroxidase antibody, (Sigma, A4416, 1:7500); Anti-rabbit IgG-HRP-linked antibody (Cell Signaling
700 Technology, #7074, 1:7.500] diluted in 1xPTW/1% slim milk powder for 1 hour, RT. After washing,
701 SuperSignal™ West Femto Maximum Sensitivity Substrate kit (Thermo Fisher Scientific) was used for
702 HRP-signal detection and finally signals were visualized by ChemiDoc Imaging System (BIORAD).
703 Specific protein bands were quantified in "Image J" and L-Cry was normalized to beta-Actin.

704 **Collection and analysis of spawning data**

705 Worm boxes were checked daily for mature worms. Worms which had metamorphosed into their
706 sexually mature male or female form and had left their tube to perform their nuptial dance were
707 scored as mature animals.

708 The recordings of mature animals (collected from June 1929 to June 1930 in Naples (*28, 29*)) were
709 digitalized and all months were aligned to moonphase and combined. For comparisons of these data
710 with our spawning data from the lab, we aligned the first day after full moon in nature with the last
711 day of full moon stimulus in the lab, since *Platynereis dumerilii* synchronizes its circalunar clock to the

712 moon off stimulus(*5*). For the circular analysis of spawning data, the lunar day of spawning was
713 multiplied by 12 for each worm, so that the 30 lunar days regularly distributed on the 360° circle.
714 Circular analysis of these data was performed using Oriana (Version 4.02, Kovach Computing
715 Services).

716 Phase-Shift Experiments

717 For Phase-Shift experiments, boxes with adult worms (at least 3 months old) were transferred from
718 standard light conditions (see "worm culture") to the naturalistic light systems (sun- and moonlight)
719 mounted in light-tight black shelves. Number of mature worms was recorded daily and number of
720 mature worms per day was used to calculate percentage of mature worms (one month: 100%). Data
721 were smoothened using a rolling mean with a window size of 3 days. Weekly samplings of premature
722 heads for gene expression analysis were performed at zt6 (2 heads per biological replicate) as
723 described in "RNA extraction and RT-qPCR".

724 RNA extraction and RT-qPCR

725 For RNA expression analysis, worm heads were sampled at zt6 (6 hours after light on) by first
726 anaesthetizing them for 5-10min with a 1:1 mixture of seawater and 7.5% (w/v) $MgCl_2$ solution. The
727 head was then cut behind the posterior eyes with a scalpel. 2-5 heads (depending on size) per
728 biological replicate were collected in 2ml tubes containing metal beads, immediately frozen in liquid
729 nitrogen and stored at -80°C until RNA extraction.

730 For RNA extraction, 350µl of RNAzol RT (Sigma-Aldrich) were added to the samples and lysis was
731 performed with TissueLyser II (Qiagen) at 30Hz for 2min. Afterwards, RNA was extracted using Direct-
732 zol RNA Miniprep kit (Zymo Research) following the manufacturer's instructions with additional on-
733 column DNaseI digest. RNA was eluted in 34µl of nuclease-free water.

734 Total RNA (200ng per sample) was reverse transcribed using LunaScript RT SuperMix Kit (New
735 England Biolabs). Final cDNA reactions were diluted to a final volume of 60-120 µl. qPCR reactions
736 were performed in 20µl total volume with Luna Universal qPCR Master Mix (New England Biolabs).
737 Target genes and reference controls were analysed in duplicate reactions for all samples. Plate
738 control cDNA and -RT controls were included on each plate. *cdc5* was used as reference gene (*14,*
739 *25*). Expression levels were calculated using the Δct method. Relative expression values were
740 calculated with the formula: relative expression = $2^{-\Delta ct}$.

Primer	**Sequence 5'-3'**
erp4.9_fwd	CAGAAGACCGTCACCAATGG
erp4.9_rev	CTCGGTAATCTTCAGGCTAGGA
g3bp2_fwd	TGAAATCCAGGAGGAAGTTGA

g3bp2_rev	GGAGGATCGGGAGACACTATC
cdc5_fwd	CCTATTGACATGGACGAAGATG
cdc5_rev	TTCCCTGTGTGTTCGCAAG

741 *Primers used for qPCR*

742 **Cloning of *g3bp1/2* and *ythdf1/2/3***

743 RNA from immature worm heads was extracted and reverse transcribed (see "RNA extraction and
744 RT-qPCR" for details). PCR for amplification was performed using Phusion Polymerase (NEB). After gel
745 electrophoresis, DNA was extracted using the QIAquick Gel Extraction Kit (Qiagen) according to the
746 manufacturer's instructions and cloned into pJET1.2 using the CloneJET PCR Cloning Kit
747 (ThermoScientific). Clones were sequence verified and sequences submitted to GenBank (MT795155,
748 MT795156). Following sequences were used for phylogenetic trees in S7:

Sequence	**GenBankID**
Mmu-G3BP1	P97855
Mmu-G3BP2	P97379
Hsa-G3BP1	Q13283
Hsa-G3BP2	Q9UN86
Dre-G3BP2	A1L1U3
Dre-G3BP1	Q7ZVG3
Dme-RIN	Q9NH72
Aca-G3BP	XP_005110089
Aca-G3BP	XP_005110087
Ame-G3BP	XP_623996
Cgi-G3BP	XP_011454471.1
Pma-G3BP	XP_033741132
Nve-G3BP	XP_001641827
Aqu-G3BP	XP_019860730
Pdu-G3BP1/2	MT795155

749 *GenBank IDs used for phylogenetic tree in S7B*

Sequence	**GenBankID**
Mmu-YTHDF1	P59326
Mmu- YTHDF2	Q91YT7
Mmu- YTHDF3	Q8BYK6
Hsa-YTHDF1	Q9BYJ9
Hsa-YTHDF2	Q9Y5A9
Hsa-YTHDF3	Q7Z739
Dre-YTHDF1	Q802Z0
Dre-YTHDF2	E7F1H9
Dre-YTHDF3	E7FAP0
Dme-YTHDF	Q9VBZ5
Cgi-YTHDF	XP_034317507
Ame-YTHDF	XP_624228
Aca-YTHDF	XP_005091424
Aqu-YTHDF	XP_003386824
Ami-YTHDF	XM_029351330

Pdu-YTHDF1/2/3	MT795156

750 *GenBank IDs used for phylogenetic tree in S7C*

751

752

Primer	Sequence 5'-3'
Pdu_g3bp2_F	TATCAAAGTCATGGTCATGGAAACTCCTAGC
Pdu_g3bp2_R	TTTGATGTGATCCTCAAGGCCTAGCGC
Pdu_ythdf2_F	AGAAACTGTGATGTCTGCAAGTGTAGACC
Pdu_ythdf2_R	GGGCGCCACCTAGTTGCTCTGG

753

754 jetlag EST- GenBank MW161055

755 Whole mount *in situ* Hybridisation combined with immunohistochemistry for L-Cry

756 Probes were generated *de novo* using previously cloned plasmids as template (see "Cloning of
757 *g3bp1/2* and *ythdf1/2/3").* Genes of interest were amplified via PCR using Phusion Polymerase (NEB)
758 and primers for pJET 1.2 with an overhang of Sp6 promoter. PCR product was purified following the
759 protocol for "QIAquick PCR Purification Kit" (Qiagen). Agarose gel electrophoresis showed right
760 amplicon sizes and single bands. For the in vitro transcription, 1µg of linearized template was used.
761 Riboprobes were labelled with anti-Digoxigenin UTPs (Roche Diagnostics) and transcribed with Sp6
762 polymerase at 37°C for 4h. Probes were purified according to the "RNeasy Kit" (QIAGEN) and eluted
763 in 40ul RNase-free water. 600-1000ng of the riboprobes were used.

764 Whole-mount *in situ* Hybridisation was carried out on premature worms of the RE strain, following
765 published procedures (*47, 50*) with adjustments made to combine it with L-Cry
766 immunohistochemistry. Worm heads were fixed in 4% PFA for 2h at RT while shaking. Proteinase K
767 digest: 5min, during which samples were very slightly rocked. After blocking in 5% sheep serum/1X
768 PTW, worm heads were incubated with the monoclonal L-Cry antibodies (5E3-3E6-E8 diluted 1:100
769 and 4D4-3E12-E7 diluted 1:50), anti-Digoxigenin-AP coupled antibody (Roche Diagnostics) and sheep
770 serum diluted to 2.5% with 1xPTW for 36-40h at 4°C, shaking. After detection using NBT/BCIP,
771 samples were incubated in the secondary antibody Alexa Fluor-488 goat anti-mouse IgG (Thermo
772 Fisher Scientific), 1:400 (36-40h at 4°C, shaking), washed in 1xPTW and mounted in DABCO/Glycerol.
773 Imaging was done using Axioplan Z2 Microscope (Carl Zeiss) with AxioCam MRc5 colour CCD camera
774 (Carl Zeiss) and captured using ZenPro Software (Carl Zeiss). The images were edited with either
775 ImageJ or Photoshop CC.

Treatment with C108 Compound

Premature *l-cry +/+* worms were kept in isolated shelves with 16:8 circadian light-dark regime and dim-moonlight conditions corresponding to the circalunar light schedule (8 nights of FM). Toxicity tests were conducted using increasing concentrations of the G3BP2 inhibitor, Compound C108 (Sigma Aldrich)(*31*). Comparison between the different concentrations showed reliable effects using 10uM of the drug while health and behaviour of worms overall seemed to be unaffected. Five days prior to taking the samples, cohorts of worms were treated with 10µM Compound C108 (Sigma-Aldrich). Control worms were cultured in parallel and treated with corresponding amounts of DMSO. Sampling (at zt6, two heads per biological replicate) and RT-qPCR was performed as described in "RNA extraction and RT-qPCR".

Statistical Analysis

All data analysis was conducted using R 3.6.1(*43*), GraphPad Prism 8.4.2, Oriana 4.02 and Microsoft Excel 2010.

Acknowledgements:

We thank the members of the Tessmar-Raible and Wolf groups for discussions. Andrej Belokurov and Margaryta Borysova for excellent worm care at the MFPL aquatic facility. We are grateful for support by the IMB Protein Production and Proteomics Core Facilities (mass spec instrument funded by DFG INST 247/766-1 FUGG). In particular, we wish to thank Dr. Mario Dejung of the Proteomics Core Facility for carrying out preliminary mass spec data analysis. We would like to thank Dr Svenja Morsbach and Beate Müller from the Max Planck Institute for Polymer Research for helping with HPLC experiment and Prof Dr Elmar Jaenicke from University of Mainz for help with SEC-MALS.

Funding

K.T-R. received funding for this research from the European Research Council under the European Community's Seventh Framework Programme (FP7/2007–2013) ERC Grant Agreement 337011 and the Horizon 2020 Programme ERC Grant Agreement 819952, the research platform 'Rhythms of Life' of the University of Vienna, the Austrian Science Fund (FWF, http://www.fwf.ac.at/en/): SFB F78 and the HFSP () research grant (#RGY0082/2010). S.K. is a recipient of a DFG fellowship through the Excellence Initiative by the Graduate School Materials Science in Mainz (GSC 266). None of the funding bodies was involved in the design of the study, the collection, analysis, and interpretation of data or in writing the manuscript.

References:

1. H. M. Fox, Lunar periodicity in Reproduction. *Proceedings of the Royal Society of London* **Series B 95**, 523-550 (1924).

2. O. Levy *et al.*, Light-responsive cryptochromes from a simple multicellular animal, the coral *Acropora millepora*. *Science* **318**, 467-470 (2007).
3. H. Numata, B. Helm, *Annual, lunar, and tidal clocks : patterns and mechanisms of nature's enigmatic rhythms*. (Springer, Tokyo ; New York, 2014), pp. xii, 360 pages.
4. P. Korringa, Relations between the moon and periodicity in the breeding of marine animals. *Ecological Monographs* **17**, 347-381 (1947).
5. C. Hauenschild, Lunar periodicity. *Cold Spring Harb. Symp. Quant. Biol.* **25**, 491-497 (1960).
6. K. Tessmar-Raible, F. Raible, E. Arboleda, Another place, another timer: Marine species and the rhythms of life. *Bioessays* **33**, 165-172 (2011).
7. V. S. Bézy *et al.*, Mass-nesting events in olive ridley sea turtles: environmental predictors of timing and size. *Anim. Behav.* **163**, 85-94 (2020).
8. G. Norevik, S. Akesson, A. Andersson, J. Backman, A. Hedenstrom, The lunar cycle drives migration of a nocturnal bird. *PLoS Biol.* **17**, e3000456 (2019).
9. L. Casiraghi *et al.*, Moonstruck sleep: Synchronization of human sleep with the moon cycle under field conditions. *Sci Adv* **7**, (2021).
10. C. Helfrich-Forster *et al.*, Women temporarily synchronize their menstrual cycles with the luminance and gravimetric cycles of the Moon. *Sci Adv* **7**, (2021).
11. T. Shlesinger, Y. Loya, Breakdown in spawning synchrony: A silent threat to coral persistence. *Science* **365**, 1002-1007 (2019).
12. D. Neumann, Temperature compensation of circasemilunar timing in the intertidal insect *Clunio*. *Journal of Comparative Physiology A - Sensory Neural and Behavioral Physiology* **163**, 671-676 (1988).
13. H.-D. Franke, The Role of Light and Endogenous Factors in the Timing of the Reproductive Cycle of Typosyllis prolifera and Some Other Polychaetes. *Am. Zool.* **26**, 433-445 (1986).
14. J. Zantke *et al.*, Circadian and Circalunar Clock Interactions in a Marine Annelid. *Cell Reports* **5**, 99-113 (2013).
15. H. D. Franke, On a clocklike mechanism timing lunar-rhythmic reproduction inTyposyllis prolifera (Polychaeta). *Journal of Comparative Physiology A: Neuroethology, Sensory, Neural, and Behavioral Physiology* **156**, 553-561 (1985).
16. F. Raible, H. Takekata, K. Tessmar-Raible, An Overview of Monthly Rhythms and Clocks. *Frontiers in Neurology* **8**, (2017).
17. C. Hauenschild, Über das lunarperiodische Schwärmen von *Platynereis dumerilii* in Laboratoriumszuchten. *Naturwissenschaften* **41**, 556-557 (1954).
18. K. Fukunaga, F. Yamashina, Y. Takeuchi, C. Yamauchi, A. Takemura, Moonlight is a key entrainer of lunar clock in the brain of the tropical grouper with full moon preference. *BMC Zoology* **5**, 11 (2020).
19. M. Fukushiro *et al.*, Lunar phase-dependent expression of cryptochrome and a photoperiodic mechanism for lunar phase-recognition in a reef fish, goldlined spinefoot. *PLoS ONE* **6**, e28643 (2011).
20. A. K. Brady, B. L. Willis, L. D. Harder, P. D. Vize, Lunar Phase Modulates Circadian Gene Expression Cycles in the Broadcast Spawning Coral Acropora millepora. *Biol. Bull.* **230**, 130-142 (2016).
21. A. Berndt *et al.*, A novel photoreaction mechanism for the circadian blue light photoreceptor *Drosophila* cryptochrome. *J. Biol. Chem.* **282**, 13011-13021 (2007).
22. V. B. Veedin Rajan *et al.*, Seasonally relevant UVA light alters neurohormone amounts and behavior via a ciliary opsin in a marine mass spawning annelid. *Nature Ecology & Evolution*, (2021).
23. S. Bannister *et al.*, TALE Nucleases mediate efficient, heritable genome modifications in the marine annelid *Platynereis dumerilii*. *Genetics* **197**, 19-31 (2014).
24. B. Xu, X. Feng, R. D. Burdine, Categorical data analysis in experimental biology. *Dev. Biol.* **348**, 3-11 (2010).
25. S. Schenk *et al.*, Combined transcriptome and proteome profiling reveals specific molecular brain signatures for sex, maturation and circalunar clock phase. *Elife* **8**, (2019).

26. T. Ayers, H. Tsukamoto, M. Gühmann, K. Tessmar-Raible, A Go-type Opsin mediates the Shadow Reflex in the annelid Platynereis dumerilii. *BMC Biol.* **16**, 41 (2018).
27. M. Guehmann *et al.*, Spectral Tuning of Phototaxis by a Go-Opsin in the Rhabdomeric Eyes of Platynereis. *Curr. Biol.* **25**, 2265-2271 (2015).
28. S. Ranzi, Ricerche sulla biologia sessuale degli Anellidi. *Pubbl. Staz .Zool. Napoli* **11**, 271-292 (1931).
29. S. Ranzi, Maturita sessuale degli Anellidi e fasi lunari. . *Boll. Soc. Ital. Biol. Sperim.* **6**, 18 (1931).
30. J. Zantke, S. Bannister, V. B. Veedin Rajan, F. Raible, K. Tessmar-Raible, Genetic and Genomic Tools for the marine annelid *Platynereis dumerilii. Genetics* **197**, 9-31 (2014).
31. N. Gupta *et al.*, Stress granule-associated protein G3BP2 regulates breast tumor initiation. *Proc. Natl. Acad. Sci. U. S. A.* **114**, 1033-1038 (2017).
32. N. Peschel, K. F. Chen, G. Szabo, R. Stanewsky, Light-Dependent Interactions between the Drosophila Circadian Clock Factors Cryptochrome, Jetlag, and Timeless. *Curr. Biol.* **19**, 241-247 (2009).
33. U. Alam, D. Kennedy, Rasputin a decade on and more promiscuous than ever? A review of G3BPs. *Biochim Biophys Acta Mol Cell Res* **1866**, 360-370 (2019).
34. J. D. Laver *et al.*, The RNA-Binding Protein Rasputin/G3BP Enhances the Stability and Translation of Its Target mRNAs. *Cell Rep* **30**, 3353-3367 e3357 (2020).
35. S. Zaccara, S. R. Jaffrey, A Unified Model for the Function of YTHDF Proteins in Regulating m(6)A-Modified mRNA. *Cell* **181**, 1582-1595 e1518 (2020).
36. B. Collins, E. O. Mazzoni, R. Stanewsky, J. Blau, Drosophila CRYPTOCHROME is a circadian transcriptional repressor. *Curr. Biol.* **16**, 441-449 (2006).
37. A. Abakir *et al.*, N(6)-methyladenosine regulates the stability of RNA:DNA hybrids in human cells. *Nat. Genet.* **52**, 48-55 (2020).
38. U. Kubitscheck, J.-P. Siebrasse, Kinetics of transport through the nuclear pore complex. *Semin. Cell Dev. Biol.* **68**, 18-26 (2017).
39. A. Czarna *et al.*, Structures of Drosophila Cryptochrome and Mouse Cryptochrome1 Provide Insight into Circadian Function. *Cell* **153**, 1394-1405 (2013).
40. N. S. Häfker, K. Tessmar-Raible, Rhythms of behavior: are the times changin'? *Curr. Opin. Neurobiol.* **60**, 55-66 (2020).
41. G. Andreatta, K. Tessmar-Raible, The Still Dark Side of the Moon: Molecular Mechanisms of Lunar-Controlled Rhythms and Clocks. *J. Mol. Biol.*, (2020).
42. P. Oliveri *et al.*, The Cryptochrome/Photolyase Family in aquatic organisms. *Marine Genomics* **14**, 23-37 (2014).
43. R. C. Team, in *R Foundation for Statistical Computing*. (https://www.R-project.org/ Vienna, Austria, 2016).
44. J. Cox, M. Mann, MaxQuant enables high peptide identification rates, individualized p.p.b.-range mass accuracies and proteome-wide protein quantification. *Nat. Biotechnol.* **26**, 1367-1372 (2008).
45. J. L. Hsu, S. Y. Huang, N. H. Chow, S. H. Chen, Stable-isotope dimethyl labeling for quantitative proteomics. *Anal. Chem.* **75**, 6843-6852 (2003).
46. C. Hauenschild, A. Fischer, "Platynereis dumerilii. Mikroskopische Anatomie, Fortpflanzung, Entwicklung. [Platynereis dumerilii. Microscopical anatomy, reproduction and development] " *Großes Zoologisches Praktikum Heft.* (Stuttgart, 1969).
47. K. Tessmar-Raible, P. R. Steinmetz, H. Snyman, M. Hassel, D. Arendt, Fluorescent two-color whole mount in situ hybridization in Platynereis dumerilii (Polychaeta, Annelida), an emerging marine molecular model for evolution and development. *Biotechniques* **39**, 460, 462, 464 (2005).
48. J. Schindelin *et al.*, Fiji: an open-source platform for biological-image analysis. *Nat. Methods* **9**, 676-682 (2012).
49. C. Stringer, T. Wang, M. Michaelos, M. Pachitariu, Cellpose: a generalist algorithm for cellular segmentation. *Nat. Methods* **18**, 100-106 (2021).

915 50. B. Backfisch *et al.*, Stable transgenesis in the marine annelid *Platynereis dumerilii* sheds new
916 light on photoreceptor evolution. *Proc Natl Acad Sci USA* **110**, 193-198 (2013).

917